의학박사 학위논문

Radiation-Induced Somatic Mutations by Whole Genome Sequencing from Normal Organoids

방사선에 의해 유도된 정상 오가노이드 내 체성돌연변이에 대한 전장유전체 분석

2019년 2월

서울대학교 융합과학기술대학원
분자의학 및 바이오제약학과
권 현 우

Radiation-Induced Somatic Mutations by Whole Genome Sequencing from Normal Organoids

지도교수 이 동 수

이 논문을 의학박사 학위논문으로 제출함

2018년 10월

서울대학교 융합과학기술대학원

분자의학 및 바이오제약학과

권 현 우

권현우의 의학박사 학위논문을 인준함

2019년 1월

위 원 장 고 태우 (인)

부위원장 이 동수 (인)

위 원 천 기정 (인)

위 원 한 도원 (인)

위 원 주 영석 (인)

Abstract

Radiation-Induced Somatic Mutations by Whole Genome Sequencing from Normal Organoids

Hyun Woo Kwon

Department of Molecular Medicine and Biopharmaceutical Science,

Graduate School of Convergence Science and Technology,

Seoul National University

Purpose:

The aim of our study was to analyze the mutational signatures induced by gamma-radiation and its possible correlation with radiation-induced carcinogenesis. For measuring somatic mutational load in the genomes of cells, 3D organoid culture technique is adapted with normal mouse pancreas and breast adult stem cells (ASCs). Quantification of DNA damages by ionizing radiation (IR) is assessed by de novo whole genome sequencing (WGS) techniques.

Materials and methods:

ASCs in pancreas duct and mammary fat pad were isolated from normal C57BL/6 female mice. *In vitro* 3D organoid cultures of ASCs were performed using tissue-specific growth factor cocktails. Clonal organoid lines were generated by expansion

of single organoid. For irradiation, cultured organoids were dissociated and irradiated under various dose (1-10 Gy) of gamma-ray using gamma-irradiator. Viability assay for IR were performed. After irradiation, organoids were dissociated as single cells using flow cytometry and cultured. Clonal irradiated organoids were established by expansion of single irradiated organoid. WGS of mouse germline, clonal ancestor organoid and irradiated organoids were performed using Illumina sequencers to a depth of 30× coverage. Clonality of organoids were determined using quantitation of organoid-specific single nucleotide variations (SNVs). The pipelines for analyzing copy number variations of chromosomal arm level, structural variations (SVs), small insertion and deletions (indels), double nucleotide variations (DNVs) and clustered mutations were constructed. Temporal change of Transcriptomes were evaluated using pancreas organoid at 0 h, 30 min, 2 h, 6 h and 24 h after 2Gy irradiation. Expression of significant radiation-responsible genes were monitored and pathway analysis for detecting radiation-induced cell response was performed.

Results:

Organoids of normal mouse pancreas and breast were successfully established. Clonal organoid lines were generated and confirmed. The survival rate of organoids showed IR dose-dependent relationship. Breast organoids showed relative radiosensitive feature which was approximate lethal dose of 50% survival (LD50) around 1 Gy than pancreas organoids (approximate LD50 around 4 Gy). Among the 6 samples, 1 of 2 Gy-irradiated organoid showed one copy loss of chromosome 4. The total amount of SVs increased with dose-dependent manner and abruptly increased over 2 Gy. Balanced-type SVs which are regarded as IR-related form were frequently noted in high-dose ($\geq$2 Gy) irradiated organoids. The amount of SNVs showed no significant relationship with irradiation in pancreas samples. However,

the amount of DNVs increased with dose-dependent manner. Small indels located in non-replicative genome area tended to be more frequent in high-dose (≥ 2Gy) samples. Mutational signatures based on clustered mutations characterized by C>T mutations. Critical genes involving DNA repair pathway including non-homologous end-joining pathway were activated after 2 h of 2 Gy irradiation. On pathway analysis, DNA repair mechanism was activated (normalized enrichment score 1.41, FDR q value 0.060). Furthermore, myc-target pathway was also enriched (normalized enrichment score 2.08, FDR q value <0.01) which might be related to increase of genomic instability.

Conclusions:

3D Organoid cultures for tissue-specific ASCs were adapted for studying gamma radiation-induced somatic mutations. The pancreas and breast organoids showed different survival rates in IR. IR-related chromosomal SVs including deletion, balanced inversion, translocation and complex SVs were found in irradiated organoid genome with dose-dependent manner. IR-induced clustered DNA damages such as DNVs could be represented as mutational signatures by IR. Future studies for analyzing IR-induced somatic mutation could reveal the mechanism of radiation-induced carcinogenesis in human body.

Keywords: Organoid, adult stem cells, gamma ray, whole genome sequencing, somatic mutation, chromosome, structural variation.

Student Number : 2015-30714

Contents

List of Figures.

List of Tables.

List of abbreviations

Abbreviations	*Full name*
IR	Ionizing Radiation
SSB	Single Strand Break
DSB	Double Strand Break
HR	Homologous Recombination
NHEJ	Non-homologous End-Joining
ASCs	Adult Stem Cells
WGS	Whole Genome Sequencing
AdDF	Advanced Dulbecco's Modified Eagle Medium:Nutrient Mixture F-12
FACS	Fluorescence Activated Cell Sorter
EGF	Epidermal Growth Factor
FGF	Fibroblast Growth Factor
PBS	Phosphate-Buffered Saline
BSA	Bovine-Serum Albumin
PI	Propidium Iodide
PCR	Polymerase Chain Reaction
SNV	Single Nucleotide Variant
DNV	Double Nucleotide Variant
VAFs	Variant Allele Frequencies
SV	Structural Variation
LD50	Lethal Dose for 50% survival
Cs-137	Cesium-137
CNV	Copy Number Variation

bp	base-pair
Rb	Retinoblastoma
Indel	Insertion and deletion
MMEJ	Microhomology-mediated end-joining
ATP	Adenosine triphosphate
A	Adenine
T	Thymine
G	Guanine
C	Cytosine
PCA	Principal component analysis
GAPDH	Glyceraldehyde 3-phosphate dehydrogenase

Introduction

Ionizing radiation (IR) has been known as the first environmental factor inducing mutagenesis and pancarcinogenesis (1, 2). The risk of cancer development by IR exhibits a dose-response relationship, and there has been considered as no safe limits for IR exposure (3). Epidemiological studies of Japanese survivors of the atomic bombing has been reported the strong evidence of relationship between IR exposure and hematologic malignancies as well as solid cancers (4-6).

The biologic effect of IR can be classified as two types: 1) Deterministic effects which severity of hazard increases with dose and practical threshold presents 2) Stochastic effects which severity of hazard is independent of dose and practical threshold dose doesn't exist(7). Cancer (especially solid cancer) has been known as stochastic effects of IR. However, leukemia (especially myeloid subtype) has been known as more likely due to deterministic effects. Additionally, the latent period presents which is the time interval between IR exposure and the appearance of a malignancy. Usually, solid cancer shows a long latency period from 10 to 60 years. These findings suggest that IR-induced carcinogenesis is hard to specify in real cases. IR-induced carcinogenesis is mixed with cancer type, ethnicity of patient, exposure amount and exposure time.

IR induce cancer by increasing the mutation that activate proto-oncogenes and/or inactive tumor suppressor genes in somatic cells. These mutations are the results of chromosomal alterations including translocations, inversions, deletions and chromosomal rearrangements (8). IR produces a unique pattern of DNA damage called "clustered damages" which are error-prone to be repaired. These types of DNA damages include double strand break (DSB), oxidized purine and pyrimidine clusters and abasic clusters (9, 10). Also, single strand breaks could be turned into the lethal DSBs when two single-strand breaks are formed in opposing strands. These

types of complex DNA damages could be revealed from the handful studies of protein-coding genes, cytogenetic assay and low-resolution genetic analysis (11-13).

DSB caused by IR has to be repaired by two principal repair pathways, non-homologous direct end joining (NHEJ) and homology-directed DNA repair (HR), that employ separate enzyme complexes. HR requires an undamaged DNA template containing a homologous sequence on the sister chromatid in the S/G_2 phases of the cell cycle. On the other hand, NHEJ does not require a DNA template and complete homologies between the rejoining ends, and works in G_1 phase of the cell cycle. NHEJ are more error-prone and related to impaired DNA replication, genomic instability and cancer development (14). Mutations resulted by NHEJ has been known to be more radiation-sensitive than mutations in HR genes, which implies that NHEJ is the dominant pathway for the removal of IR-induced DSBs. However, both the HR and NHEJ repair mechanisms could contribute to genomic instability (15). Therefore, more comprehensive analysis of mutations induced by IR is needed to reveal the relationship between IR and carcinogenic mutagenesis. Moreover, approach for analyzing clustered mutations uses mutation-containing plasmid which is challenge in analyzing mammalian cells because of different experimental context (16). So, the establishment of pipeline for analyzing somatic mutations in human cells are essential for evaluating IR-induced carcinogenesis.

Measuring the somatic mutation load in normal cell/tissue has been known as critical to understand the development of cancer, because the accumulation of mutations is regarded to underlie carcinogenesis (17). The adult stem cells (ASCs) in each specific tissues are the concern of somatic mutational accumulation, because of their capability for self-renewal and thereby transmission of mutations to daughter cells. A high turnover of DNA replication which might include cancer-driving mutations in ASCs has been related to be higher cancer incidence (18-20). Therefore, IR-induced mutations accumulated in ASCs need to be investigated for IR-induced

carcinogenesis.

Measuring somatic mutations in ASCs has technical challenges. Detecting the small mutational events in ASCs can be possible by sequencing monoclonal cells not by bulk sequencing of polyclonal cells. Therefore, technique for assessing single cell genome is needed. Furthermore, unbiased selection of cells is required to reveal the random mutational event in ASCs. To find a low mutational event in small population of ASCs, deep sequencing of whole genome in single ASC with removing errors and biases of sequencing is needed (21).

Recent technical advances of 3D *in vitro* culture have allowed the long-term culture of ASCs as organoid system. The advantage of organoid culture system is not only continuing self-renewal capacity of ASCs but also the maintenance of primary physiology and differential capability of tissue-specific ASCs (22). Until now, several tissue-specific organoid culture technologies have been developed under combination of growth factors and pivotal requirements (23). Also, recent study has describe the platform for culturing single ASCs as organoid and whole genome sequencing (WGS) analysis to reveal the mutation accumulation in single ASCs (24). These techniques can be also useful to reveal the mutational pattern induced by IR in ASCs.

The assessment of doses of human body from IR exposures have been developed using specific dosimetric quantities. Among them, effective dose has the central role for dose assessments in view of radiological protection. The estimated doses of human body after IR exposures is calculated by adding the dose of internal organ. Human organs and tissues differed from each other in terms of radiation sensitivity (25). Therefore, direct assessment of radiation effect by organ is essential to understand the pathomechanism of IR affecting human body. Organoid techniques can be used to establish the in vitro various tissue specific culture, and adapted to evaluate the radiation effect of particular organ directly.

Purpose

The aim of our study was to analyze the mutational signatures induced by IR and its possible correlation with IR-specific carcinogenesis. For measuring somatic mutational load in the genomes of cells, 3D organoid culture technique is adapted with two different tissue-specific ASCs (pancreas and breast). Quantitative measurement of DNA damages by IR is assessed by de novo WGS techniques. The experimental scheme is represented in Figure 1.

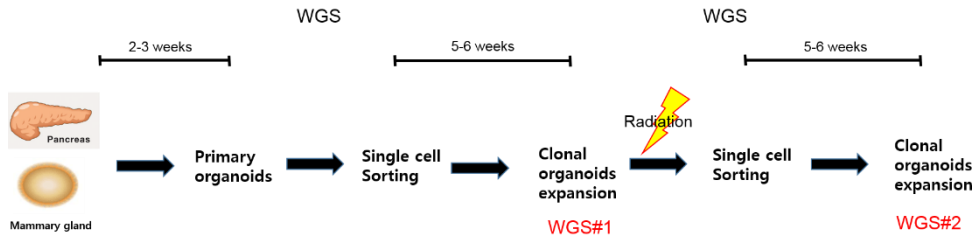

Figure 1. Schematic representation of the experimental procedure. Primary organoid cultures are derived from a mouse pancreas and mammary gland tissues, and expanded for 2-3 weeks. Subsequently, single cells are isolated using flow cytometry, and cultured to establish clonal organoid lines. The clonal organoids are expanded for ~ 6 weeks. Then the clonal organoids are irradiated, and subsequent single cell isolation was done. The irradiated clonal organoids are re-expanded for ~6 weeks. The clonality of organoids are evaluated by the whole genome sequencing (WGS) results.

Materials and Methods

Establishment of mouse organoid cultures

All animal experiments were performed under accordance with the institutional animal care and use committee at the Seoul National University. C57BL/6 female mice of 9-14 weeks old were used to obtain the primary organ tissues. After the euthanasia using CO_2, the mammary fat pad tissue, pancreas and spleen were extracted.

Pancreatic ducts were isolated using 0.125 mg/ml collagenase P (Roche) and dispase 0.125 mg/ml (Life Technologies) at 37℃. Isolated ducts were seeded with Matrigel (BD Bioscience) and cultured according to previous reports (22, 26). Culture media was based on AdDF+++ (AdDMEM/F12; Gibco, 10 mM HEPES; Gibco, 1% Glutamax; Gibco, 1% penicillin-streptomycin; Gibco) supplemented with B27 (Gibco), 1 mM N-Acetylcysteine (Sigma), 10 nM gastrin (Sigma), 10 mM nicotinamide (Sigma) and the growth factors: 50 ng/ml EGF (Peprotech), 5% Rspondin1-conditioned media (kindly provided by Hans Clevers), 25 ng/ml Noggin (Peprotech) and 100 ng/ml FGF10 (Peprotech). Medium was changed every 2-3 days and organoids were passaged every one week. For passaging, organoids were harvested and mechanically dissociated, and transferred to fresh Matrigel.

Mammary fat pad tissues were minced, washed with AdDF+++ and digested in 10 ml breast organoid media with 1.25 mg/ml collagenase (Sigma, C9407) (27). Culture media was based on AdDF+++ supplemented with B27 (Gibco), 1 mM N-Acetylcysteine (Sigma), 5 μM Y-27632 (Sigma), 500 nM A83-01 (Tocris), 500 nM SB202190 (Sigma), 5 mM nicotinamide (Sigma), 50 μg/ml primocin (invivogen) and the growth factors: 5 nM Neuregulin-1 (Peprogech), 10% Rspondin1-conditioned media, 5 ng/ml EGF (Peprotech), 100 ng/ml Noggin (Peprotech), 5 ng/ml FGF7 (Peprotech) and 20 ng/ml FGF10 (Peprotech). Medium was changed

every 2-3 days and organoids were passaged every one week. For passaging, organoids were harvested and mechanically dissociated using TrypLE (Gibco), and transferred to fresh Matrigel (Growth Factor Reduced; BD Biosciences).

Isolation and culture of mouse clonal organoids

Cultured organoids were harvested and mechanically dissociated using TrypLE. Harvested organoids were transferred to a 15-ml tube and centrifuged via 500 g at 5 min. After centrifuging, supernatants were removed and organoids were resuspended using culture media. Organoid suspension were filtered using 40 μm strainer. By using a cell sorter (BD-FACSAria II; BD Biosciences), single cells were sorted into a 15-ml tube with 2 ml of AdDF+++. Single cells were selected in the FACSDiva software on the basis of forward- and side-scatter characteristics (24). Sorted cells were seeded to Matrigel (500-1500 / well). For maintaining single pancreas organoid, 10 μM Y-27632 was added to culture media during 5 d after the single cell sort. After 2 weeks, grown organoids were picked using 200 μl pipette tip and mechanically dissociated using TrypLE. Then single organoids were seeded to 24 well plate and cultured by previously described.

Irradiation of mouse clonal organoids

After the harvest and dissociation of organoids, cell suspension were transferred into 1.5 ml Eppendorf tube. Single cells were irradiated with Cs-137 gamma irradiator (J.L. Shepherd & ass. Glendale, CA, USA) at a dose rate of 33 mGy/s (doses of 1 to 10 Gy). After the irradiation, cells were sorted using a cell sorter, and seeded to Matrigel (500-1500 / well). For RNA experiments, organoids were irradiated in well-plated status using 2 Gy.

Viability assay

Viability assay of irradiated organoids was performed to evaluate the effect of gamma irradiation by visual analysis and quantitative assay using viability assay kit (CellTiter-Glo 3D; Promega). For visual analysis, organoids were irradiated and immediately seeded to a 12 well plate (10,000 cells/well). The size and number of irradiated organoids were checked at 5 Day after seeding. For quantitative assay, dissociated single cells were irradiated and seeded to a 96 well white plate with 2 μL of Matrigel (500/well and 1000/well). At Day 5 after plating, cells were lysed and total amount in the well was measured by luminometer (1420 VICTOR LIGHT).

Cell cycle analysis

Cell cycle analysis of irradiated organoids was performed to evaluate the effect of gamma irradiation for cell cycle arrest. Organoids were dissociated as single cells using TrypLE and harvested. Cells were spin-down and washed in phosphate-Buffered Saline (PBS), and fixed in cold 70% ethanol for at least 24 hr. Then ethanol was removed after fixation, and cells were washed in PBS with 0.1 % bovine serum albumin (BSA). Washed cells were spin-down and resuspended in PBS with 0.1 % BSA. Cells were treated with ribonuclease and 13 μl Propidium Iodide (PI) was added. After 20 min of PI staining, DNA amount in single cells were analyzed via FACS sorting. 10,000 cells for pancreas and 5,000 cells for breast were counted, and each cell cycle proportion was determined in histogram plot.

Whole genome sequencing and read alignment

Genomic DNA was isolated from the clonally expanded organoids with a minimum amount of 1 μg (DNeasy blood & tissue kit; QIAGEN). DNA libraries were generated using Illumina standard protocols (TruSeq PCR-free library). The libraries were sequenced with paired-end (2 × 150 bp) runs using Illumina Hiseq X

Ten sequencers to a minimal depth of 30× base coverage. Genomic DNA isolated from spleen was used as reference genome and sequenced as same manner. Sequence reads were mapped against mouse reference genome MM10 using Burrows-Wheeler Alignment (28). Sequence reads were marked for duplicates and realigned by chromosome coordinates. Sequence read-quality scores were calculated.

RNA sequencing

Total RNA sequencing from 2 Gy-irradiated clonal pancreas organoids was performed to evaluate the temporal change of transcriptomes after radiation exposure. RNA was isolated from irradiated organoids (triplicated) at 0 h, 30 min, 2 h, 6 h and 24 h after irradiation using the RNeasy mini kit (QIAGEN). RNA libraries were generated after rRNA depletion using Illumina standard protocols with 6G output. Sequence reads were mapped against mouse reference transcriptome.

Genome and transcriptome analysis

All procedure of genomic and transcriptomic analysis was based on best practice guidelines (https://software.broadinstitute.org/gatk/best-practices/). Variant calling of somatic mutations was performed using Strelka (v1.0.14), VarScan (v2.4.1) and MuTect (v1.1.7) caller (28-30). Filtering procedures of somatic mutations were followed: we considered the positions with a base coverage of at least 10× in both the culture and the reference sample. Variant alleles that overlapped with single-nucleotide variants (SNVs) in the SNP database (dbSNP) or reference alleles were excluded (31). Positions which had at least 3 sequence reads with soft clipping were excluded (in any of variant allele or reference allele). Sequence reads with low mapping quality (<40) were excluded. Filtered somatic mutations merged to a single vcf file were visually inspected and determined as true finding. Validation of

clonality was determined by analyzing the variant allele frequencies (VAFs) of the somatic muations ≥ 0.3. Mutational signatures induced by IR were analyzed using Mutalisk toolkit (32). Clonal SNVs in irradiated samples were considered as transmitted if at least 2 reads of same SNVs were founded in ancestor genome. The copy number variations (CNVs) of chromosome arm level was searched using Sequenza tool. The amount of SNVs and double nucleotide variants (DNVs) in irradiated clonal organoids was measured to evaluate the IR dose-dependency. The structural variation (SV) was classified as duplication, deletion, insertion, inversion and translocation. In case of deletion, duplication and insertion, size >50bp was considered as SVs. The amount of SV in irradiated clonal organoids was compared with the IR dose. All detected SVs were confirmed by visual inspection using IGV viewer.

Sequence read-quality scores were checked and genes with low read counts (<10 in all samples) were removed. Resulting in a 20324 genes by 15 samples were analyzed. The temporal change of total RNA expression pattern was calculated using DESeq2 (33). Significant gene sets related to DNA repair/polymerization mechanism were selected based on GO database (http://software.broadinstitute.org/gsea/msigdb/genesets.jsp). The activation of IR-induced molecular pathway was detected using GSEA enrichment analysis. Unsupervised clustering of irradiated samples were evaluated after regularized-logarithm transformation of counts data using principal component analysis (PCA) and measuring Euclidean distance of variance between samples. The statistical significance was determined using FDR correction of nominal P value. To evaluate the change of expression amount, student's t test was used.

Results

Part I. Establishment of clonal mouse organoids

Establishment of mouse organoid cultures

We successfully established normal mouse pancreas and breast organoid lines which readily expanded (long-term self-renewal capacity was checked until 30 serial passages). Pancreas organoids were homogenous and predominantly cystic phenotype (Fig. 2, left), whereas breast organoids were relatively heterogenous and solid phenotype (Fig. 2, right).

Establishment of clonal organoids

Cultured bulk organoids were dissociated and harvested to generate a single cell suspension. The procedure of single cell sorting was 1) find a major cell population which are likely single cells (Fig. 3, left column), 2) selection of singlets on the basis of the side-scatter area (Fig. 3, middle column) and the forward-scatter area (Fig. 2, right column). The scatter pattern of pancreas and breast cells were not significantly different. After the single-cell sort, seeded organoids have grown enough to be discernible to the naked eye approximately after 2 weeks.

The clonality of expanded organoid cultures from single organoid was checked by pattern analysis of VAFs from DNA extract. Theoretical VAFs of SNVs in a clonal organoid are distributed as Gaussian distribution. And we adapt the criteria of VAF filtering threshold as 0.3 (24). In case of pancreas organoid, a total of 207,092 SNVs was found as germline mutation. Among them, 1665 SNVs were selected as organoid-specific SNVs after filtering. In histogram density plot, the peak around 0.5 of clonal heterozygous SNVs was noted which implied the clonality of the cultured organoid (Fig. 4). And there was lower VAFs

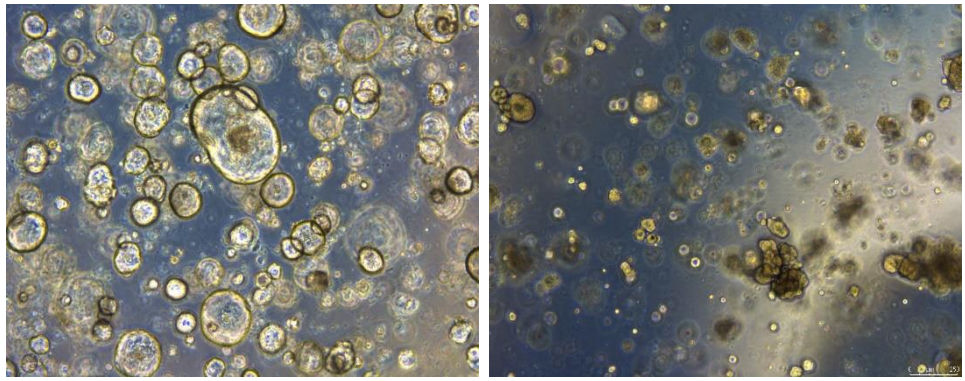

Figure 2. Microscopic images depicting pancreas (left) and breast (right) organoid morphology. Images were taken after 3 day of seeding. Scale bar, 250 μm.

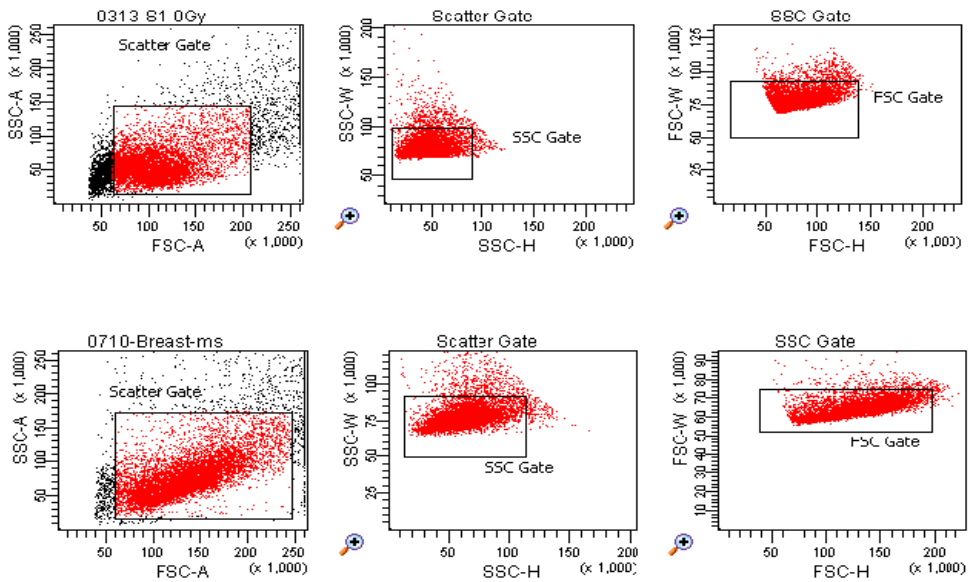

Figure 3. Flow cytometry plots for gating strategies of single cells from pancreas (upper panel) and breast (lower panel) organoid suspensions.

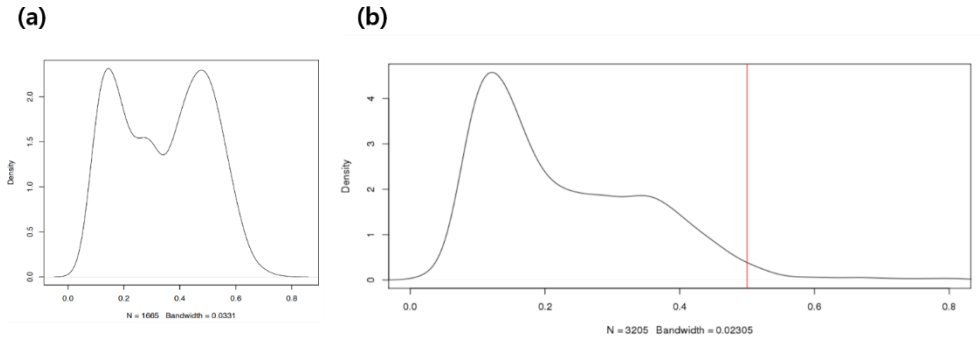

Figure 4. Variant allele frequency distribution plot for ancestor organoids. (a) Ancestor genome of pancreas organoids showed high peak on VAFs of 0.5. (b) However, ancestor genome of breast showed peak VAFs around 0.35 which means the ancestor breast organoids consisted of dominant and minor population.

subclonal mutations which might be acquired after the single organoid expansion (Fig. 4a). On the other hand, a total of 3205 SNVs were selected as organoid-specific SNVs after filtering in ancestor breast organoid genome. In histogram density plot, the peak around 0.35 of heterozygous SNVs was noted which implied the presence of dominant and minor population in ancestor breast organoid (Fig. 4b).

Part II. Irradiation of organoids

We examined the organoid viability and growth after exposure to various doses of IR. Organoids were dissociated as single cells and suspension were irradiated with 1 to 10 Gy of gamma-ray from Cs-137 line source. After the irradiation, the same number of cells was seeded at 96 well plate (500/well or 1000/well). The total amount of viable organoids per well was evaluated by measuring total amount of adenosine triphosphate (ATP) after 5 Day of seeding. Compared with the unirradiated control, the viability of organoids was significantly decreased in irradiated samples. In case of pancreas organoids, the estimated lethal dose of 50% (LD50) of IR was around 4 Gy (Fig. 5, left). On the contrary, breast organoids showed more sensitivity for IR that the estimated LD 50 was below 1 Gy (Fig. 5, right).

The growth of organoids after IR was also visually checked. The formation of pancreas organoid was not significantly changed at $\leq$ 2 Gy, but was significantly disrupted at higher doses (Fig. 6).

The effect of IR for cell cycle arrest was evaluated by estimating chromosome content of single cells. In histogram plot of chromosome amount at each cells acquired by cell sorting, the major cell population of unirradiated organoids was G_0/G_1 stage for both of pancreas (72.3 %) and breast (67.9 %) (Fig. 6 and 7). The relative numbers of G_0/G_1 cells were not significantly change according to the irradiation: 72.6, 72.4, 72.1, 71.1 % at 1, 2, 4, 8 Gy for pancreas (Fig. 7) and 66.7, 70.7, 71.5 % at 1, 2, 4 Gy for breast (Fig. 8).

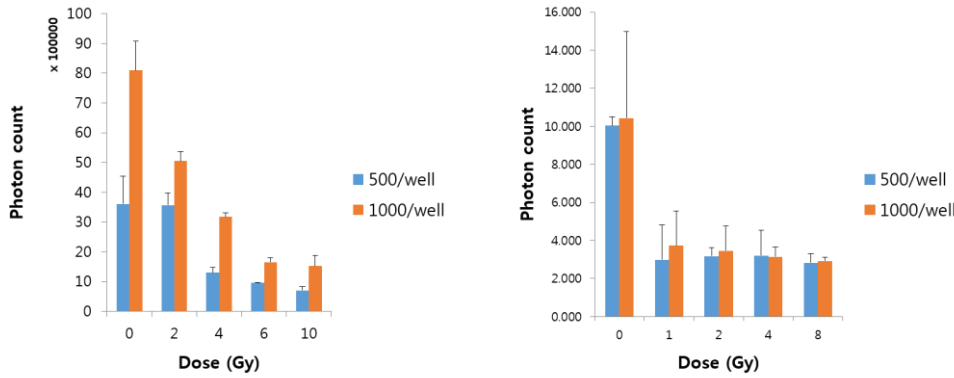

Figure 5. Growth and viability of irradiated pancreas (left) and breast (right) organoids.

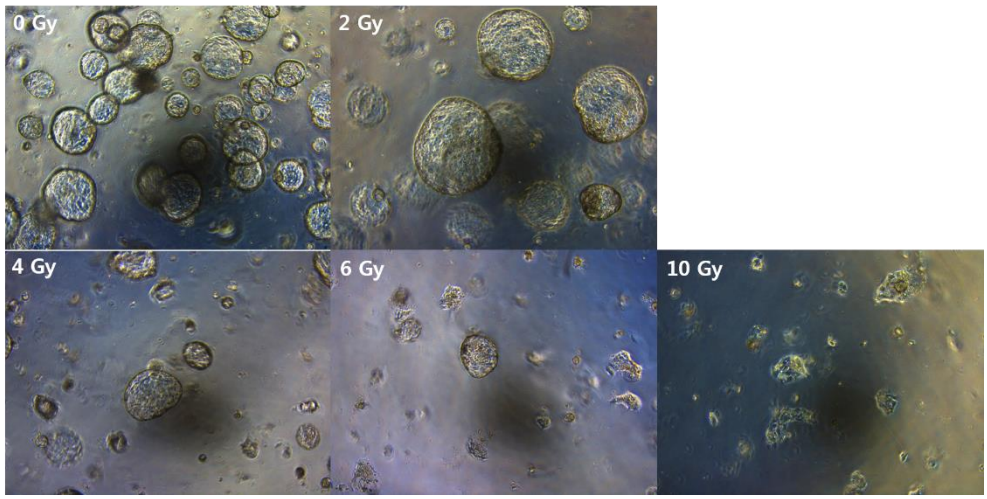

Figure 6. Microscopic images of irradiated pancreas organoids at 5 Day after irradiation.

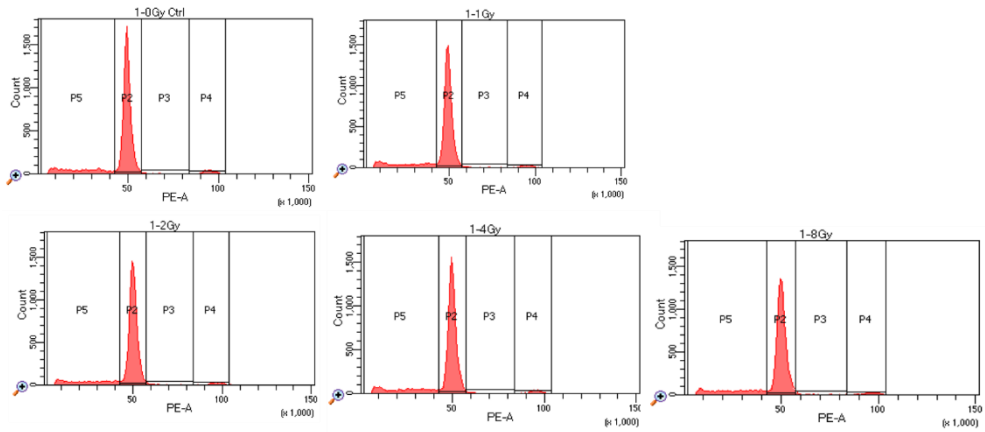

Figure 7. Histogram plots of cell cycle analysis for irradiated pancreas organoids. After irradiation, the cells were stained with propidium iodide (PI). Fluorescence activated cell sorting (FACS) analysis was performed for chromosome content measurement.

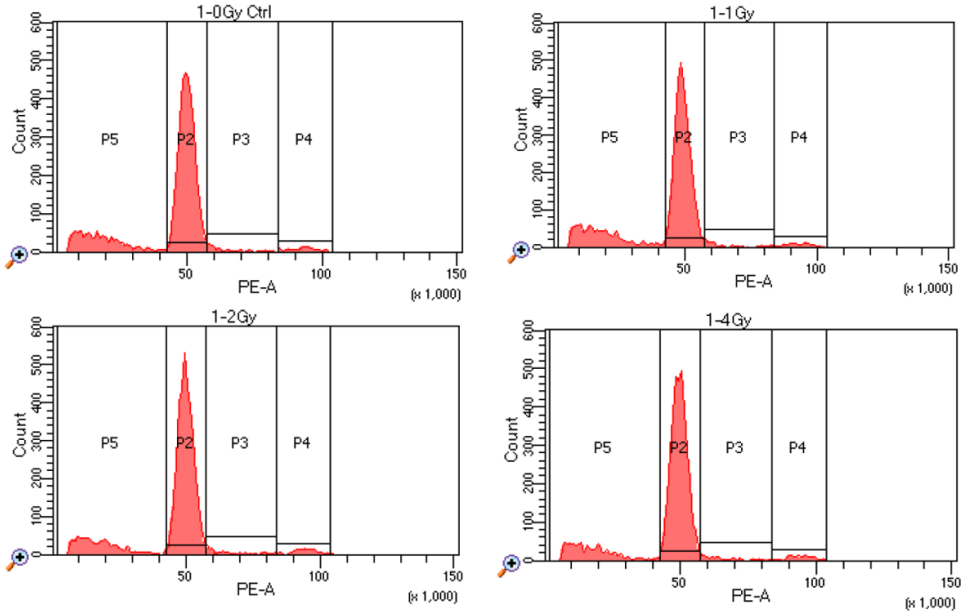

Figure 8. Histogram plots of cell cycle analysis for irradiated breast organoids.

Part III. Analysis of somatic mutations induced by IR

A total of 14 DNA samples (6 of unirradiated control, 2 of 1Gy IR, 3 of 2 Gy IR, 2 of 4 Gy IR, 1 of 8 Gy IR) from clonal pancreas organoids were analyzed. The clonality of samples were checked by distribution of VAFs (Fig. 9.) in organoid genomes. Among the analyzed samples, 9 showed peak ratio around 0.5 of VAFs which indicated clonality of samples. And a total of 20 DNA samples (3 of unirradiated control, 6 of 1 Gy IR, 8 of 2 Gy IR, 3 of 4 Gy IR) from breast organoids were also analyzed. All the analyzed samples were determined as clonal organoid genomes.

Copy number variations at chromosome arm level

Chromosome instability induced by IR was evaluated by copy number variations (CNVs) at chromosome arm level. Among the irradiated samples, 1 sample of 2 Gy-irradiated organoids showed one copy loss of chromosome 4 (Fig. 10).

Structural Variations

The quantitative mutational loads per each samples according to the IR doses were evaluated via the amount of genomic SVs. SVs were classified as 1) deletion, 2) duplication, 3) insertion, 4) inversion, 5) translocation and 6) complex SV which was resulted by more than 3 DSBs.

Among the type of SVs, duplication was mostly frequent at low-dose (≤ 1 Gy) in both of pancreas (8/9, 88.9%) and breast samples (12/17, 70.6%) (Table 1, Fig. 13). On the other hand, insertion was found only one case in pancreas samples (8 Gy-irradiated) (Fig. 14) and not found in breast organoids. Considering the mechanism of SV generation, these two types of SVs might be IR-independent.

The total number of IR-related SVs increased according to IR-dose (Table 1, Fig. 11). Among them, a majority was deletion (78.6%, 33/42). Deletion was dramatically increased over the IR dose of 2 Gy (Fig. 12). In 2 Gy-irradiated organoid genome, 1 complex SV consisted of large deletion and balanced inversion were noted (Fig. 15). 4 Gy-irradiated pancreas organoid had 1 balanced inversion (Fig. 16 and 17) and 8 Gy-irradiated sample had 1 balanced inversion and 2 balanced translocation. Balanced translocation was noted in 2 Gy- and 8 Gy-irradiated clonal organoids (Fig. 18). No copy number alteration is shown across the two breakpoints of different chromosome (Fig. 19). Finally, there is no evidence that radiation induces chromothripsis or chromoplexy.

The similar pattern of SV distribution was found in irradiated breast organoid genomes. Most frequent type of SV was deletion (14/23, 60.9%). IR-related SVs increased according to dose and abruptly increased over 2 Gy. Balanced-type SVs were found from 1 Gy-irradiated samples. Complex SVs were found over 2 Gy. Also, no definite chromothripsis or chromoplexy was found in irradiated samples.

The presence of microhomology at the breakpoint of IR-related SVs was checked for evaluating the mechanism of SV generation (34) (Fig. 11). In irradiated pancreas organoids, the presence and absence of microhomology at breakpoint was found to be similar. On the other hand, the absence of microhomology seemed to be more frequent than the presence of microhomology in irradiated breast samples.

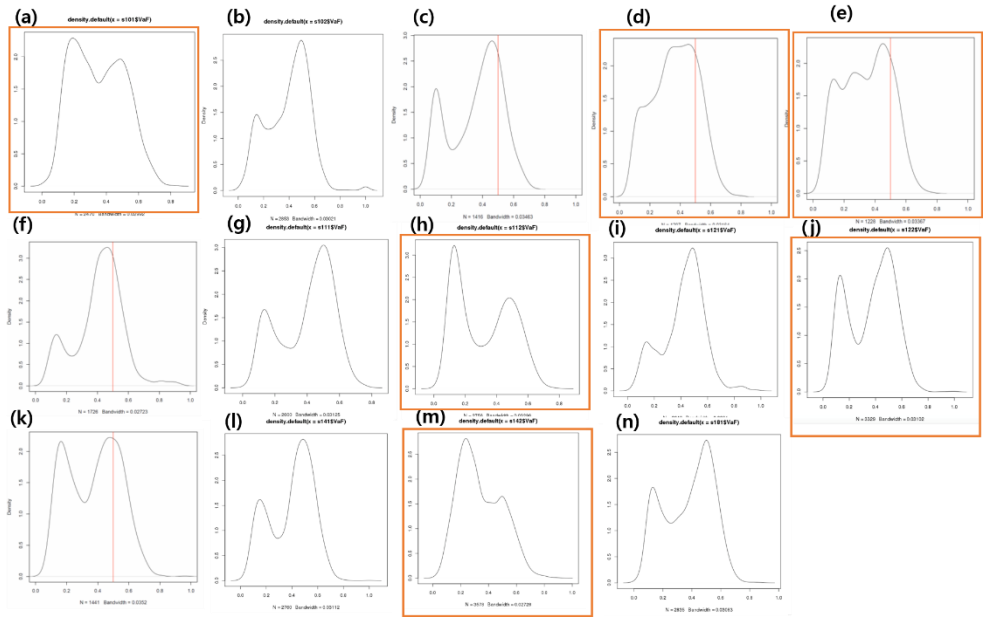

Figure 9. Distribution plots of the VAFs of somatic mutations in pancreas organoid DNA isolates from irradiation experiment. (a-f) Unirradiated control samples (g, h) 1 Gy-irradiated samples (i-k) 2 Gy-irradiated samples (l, m) 4 Gy-irradiated samples (n) 8 Gy-irradiated sample (red box: nonclonal organoids).

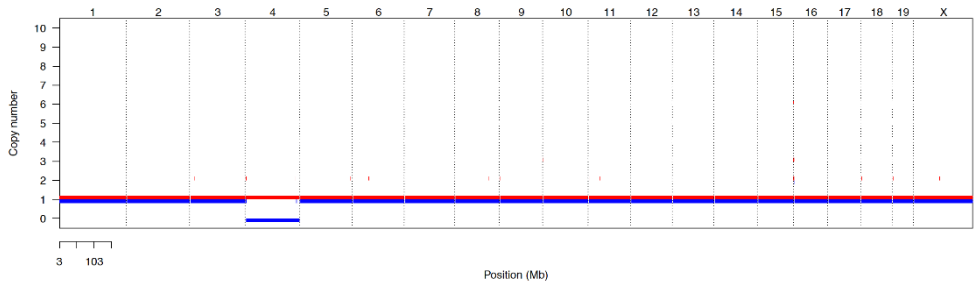

Figure 10. The change of chromosome arm level at one sample of 2 Gy irradiated pancreas organoid. One copy of chromosome 4 was loss.

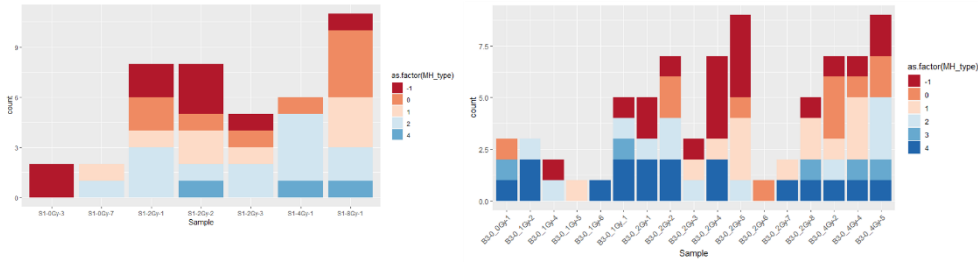

Figure 11. Relationship between IR dose and the number of structural variations (SVs).

Table 1. Summary of results for genomic structural variations induced by ionizing radiation in clonal pancreas and breast organoids

Tissue	Dose (n)	Number of structural variations (per sample)						Total	
Pancreas		deletion	duplication	insertion	inversion	translocation	complex		*
	0 Gy (3)	1.3	2.3		0.3			3.9	1.6
	1 Gy (1)		1					1	0
	2 Gy (3)	5.7	0.3		0.3	0.7	0.3	7.3	7
	4 Gy (1)	5			1			6	6
	8 Gy (1)	7		1	1	2		11	
Breast									
	0 Gy (3)	1	2					3	1
	1 Gy (6)	1.5	1		0.2	0.2		2.9	1.9
	2 Gy (8)	3.1	0.1		1.3	0.3	0.3	5.1	5
	4 Gy (3)	4.7	1.3		2.3	0.3	0.3	8.9	7.6

*excluding insertion and duplication

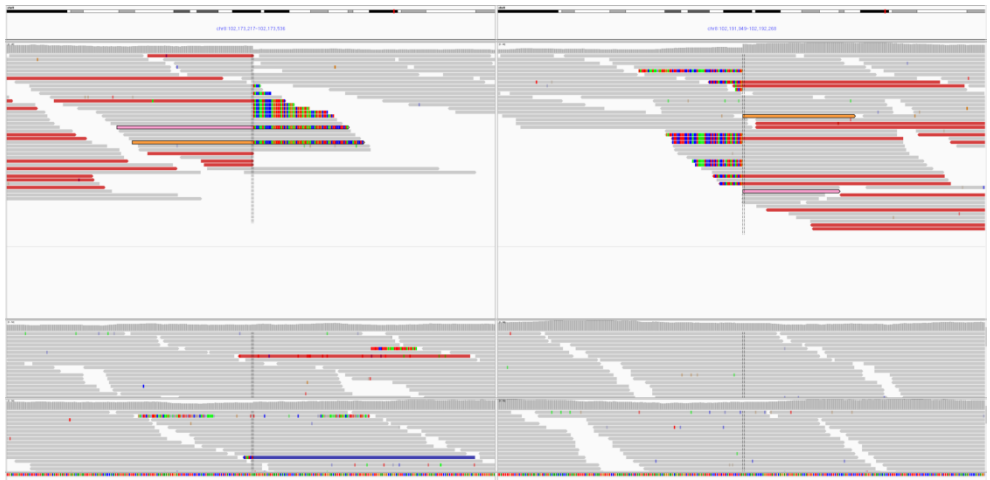

Figure 12. Representative case of a large deletion in irradiated pancreas organoid. A 18.5 kb deletion (102,173,377-102,191,931) was noted in chromosome 8 of 2Gy-irradiated organoid. Upper, irradiated sample genome; Middle, ancestor genome; lower, germline genome.

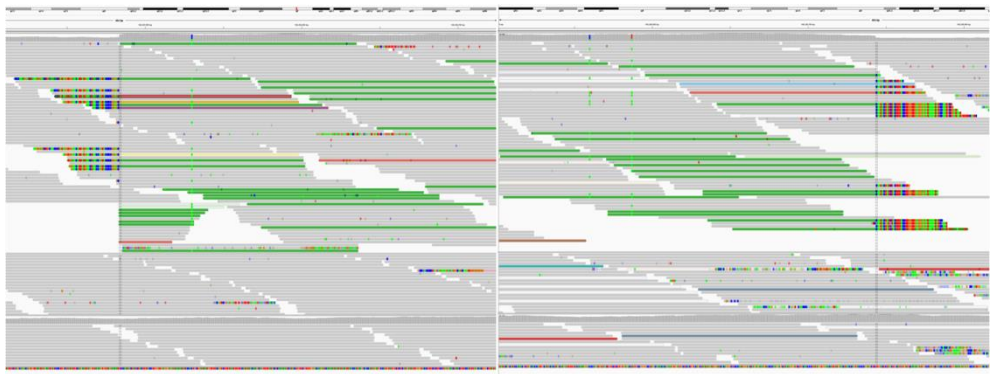

Figure 13. Case of a large duplication. A 39.9 kb duplication (143,203,884-143,243,740) was noted in chromosome 1 of 1 Gy-irradiated organoid. Upper, irradiated sample; Middle, ancestor; lower, germline genome.

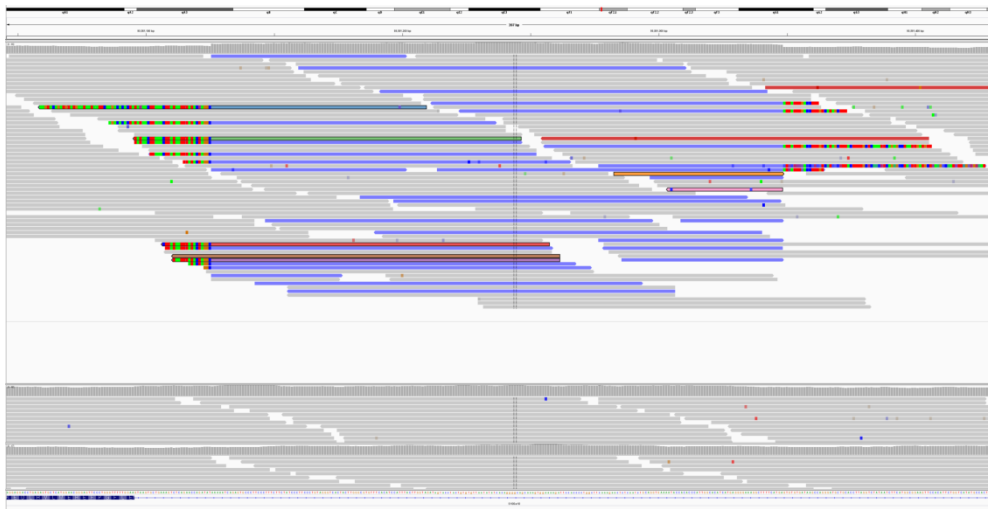

Figure 14. Case of an insertion. 225 bp-sized DNA strand (93,561,126-93,561,349) in chromosome 3 was inserted in chromosome 1 (99,908,239) of 8 Gy-irradiated organoid. Microhomology at 5' and 3' was A and GA, respectively. Upper, irradiated sample; Middle, ancestor; lower, germline genome.

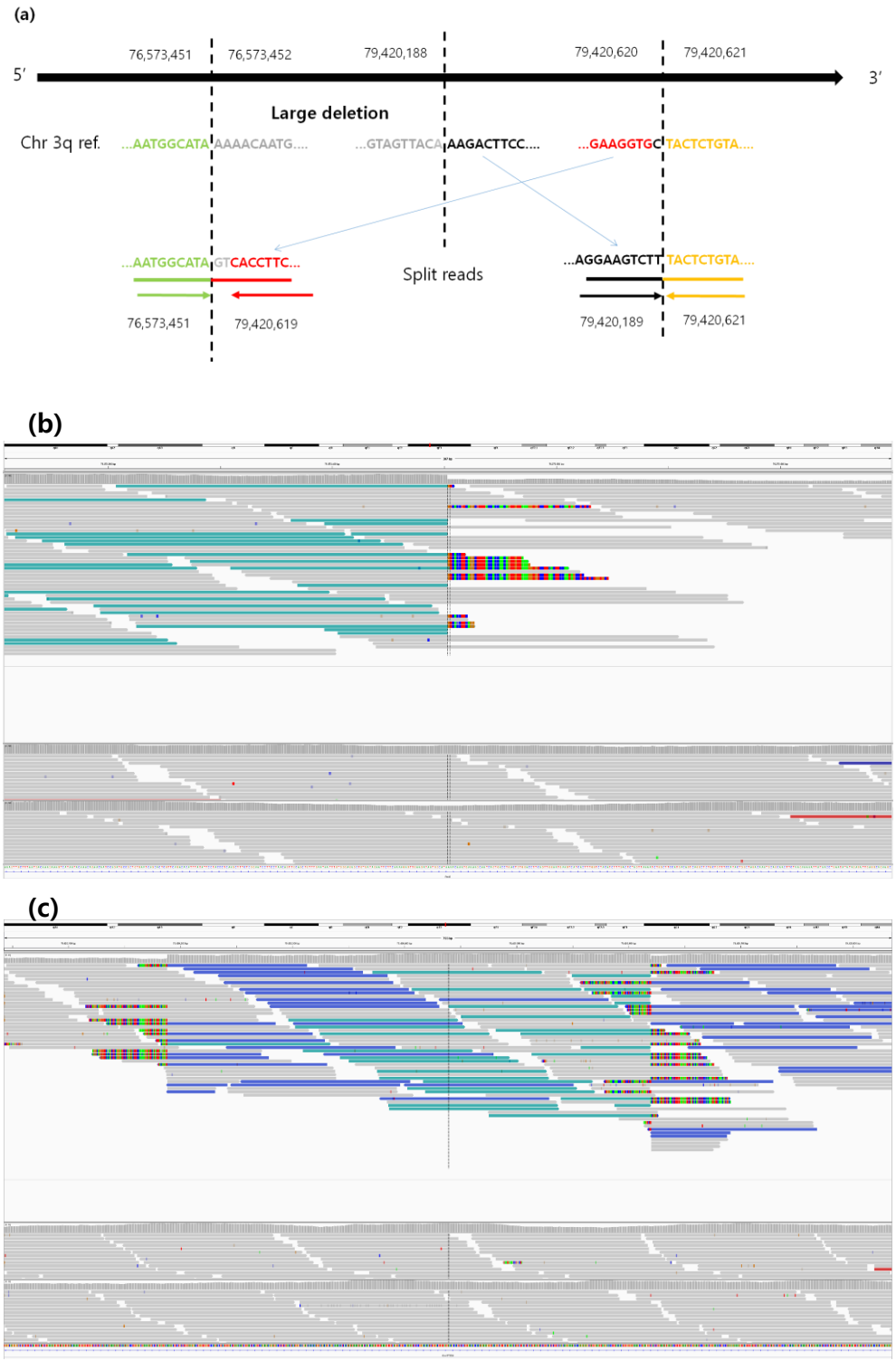

Figure 15. Case of a complex structural variation. (a) Schematic overview. A 2.8 Mb

deletion (76,573,452-79,420,188) was noted in q arm of chromosome 3 of 2 Gy-irradiated organoid, followed 430 bp balanced inversion (79,420,189-79,420,619) was seen. Rearrangement of split reads across the breakpoint (b, 5’ site of deletion; c, inversion site). Upper, irradiated sample genome; Middle, ancestor genome; lower, germline genome.

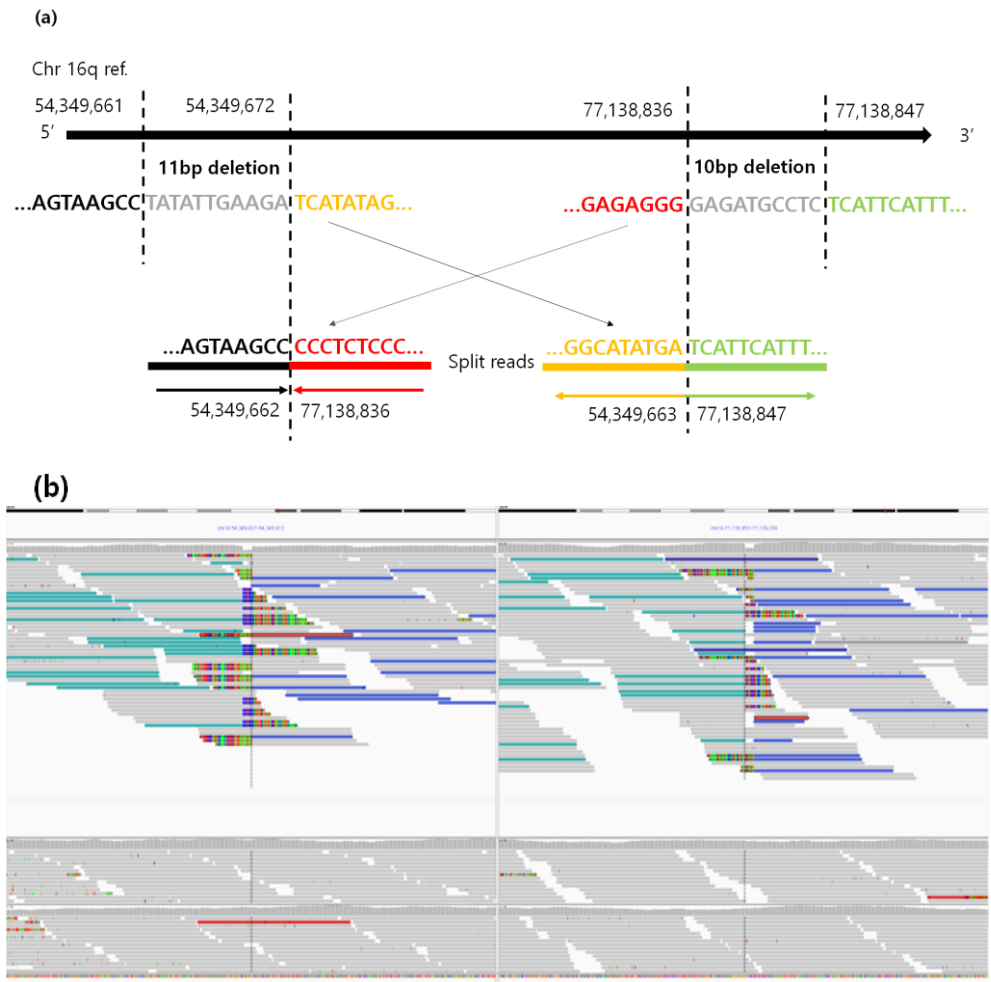

Figure 16. Representative case of a balanced inversion. (a) Schematic overview of balanced inversion. A 22.8 Mb inversion (54,349,672-77,138,836) was noted in q arm of chromosome 16 of 4 Gy-irradiated organoid. (b) Rearrangement of split reads across the breakpoint of chromosome 16. Upper, irradiated sample genome; Middle, ancestor genome; lower, germline genome.

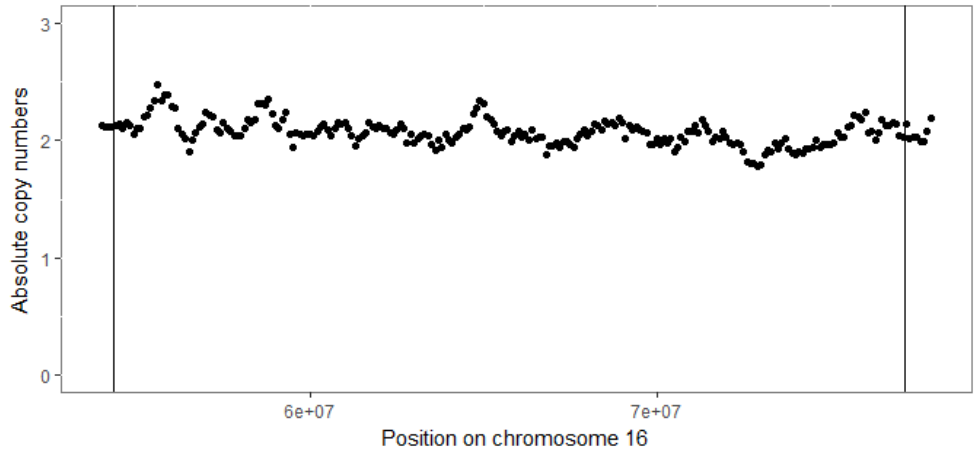

Figure 17. Copy number variations (CNVs) plot for balanced inversion site of chromosome 16 in 4 Gy-irradiated organoid. There is no alteration of copy number in balanced inversion site. Vertical line: breakpoint on chromosome.

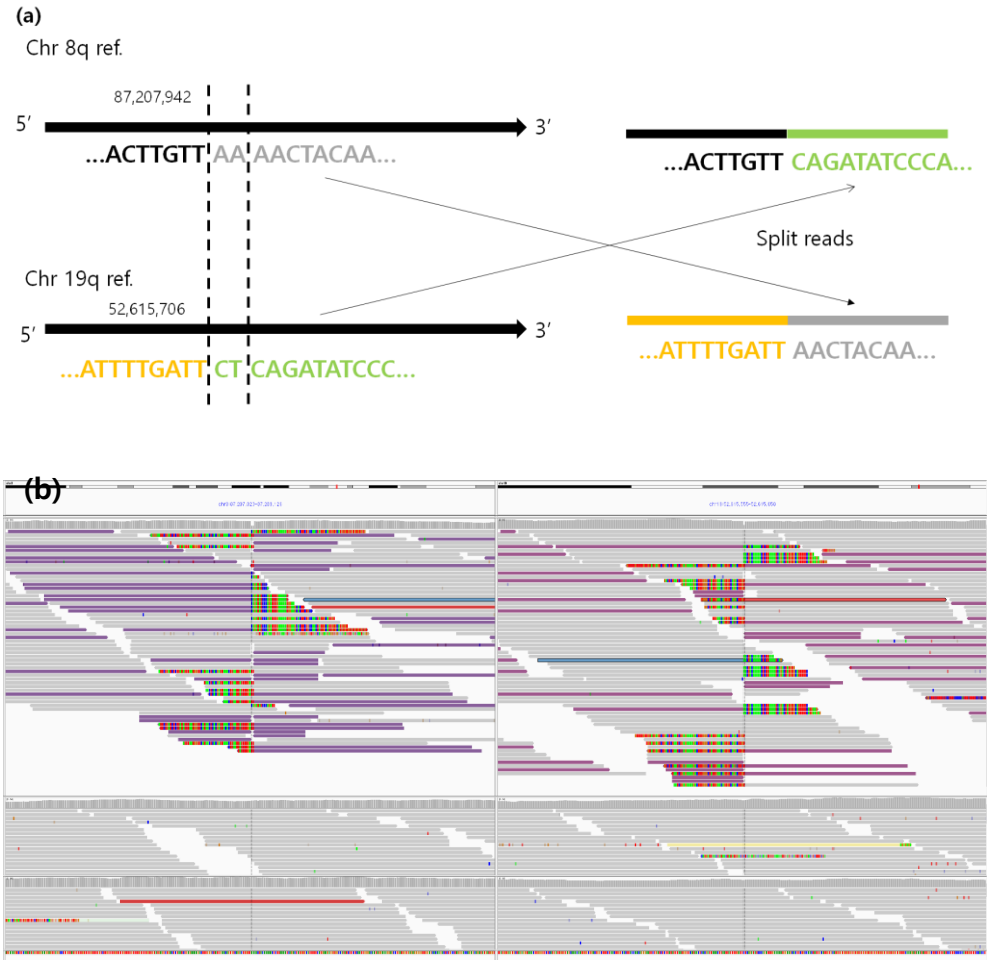

Figure 18. Representative case of a balanced translocation. (a) Schematic overview. (b) Rearrangement of split reads across the breakpoint of chromosome 8 (left) and 19 (right) of 2 Gy-irradiated sample. Upper, irradiated sample; Mid, ancestor; lower, germline genome.

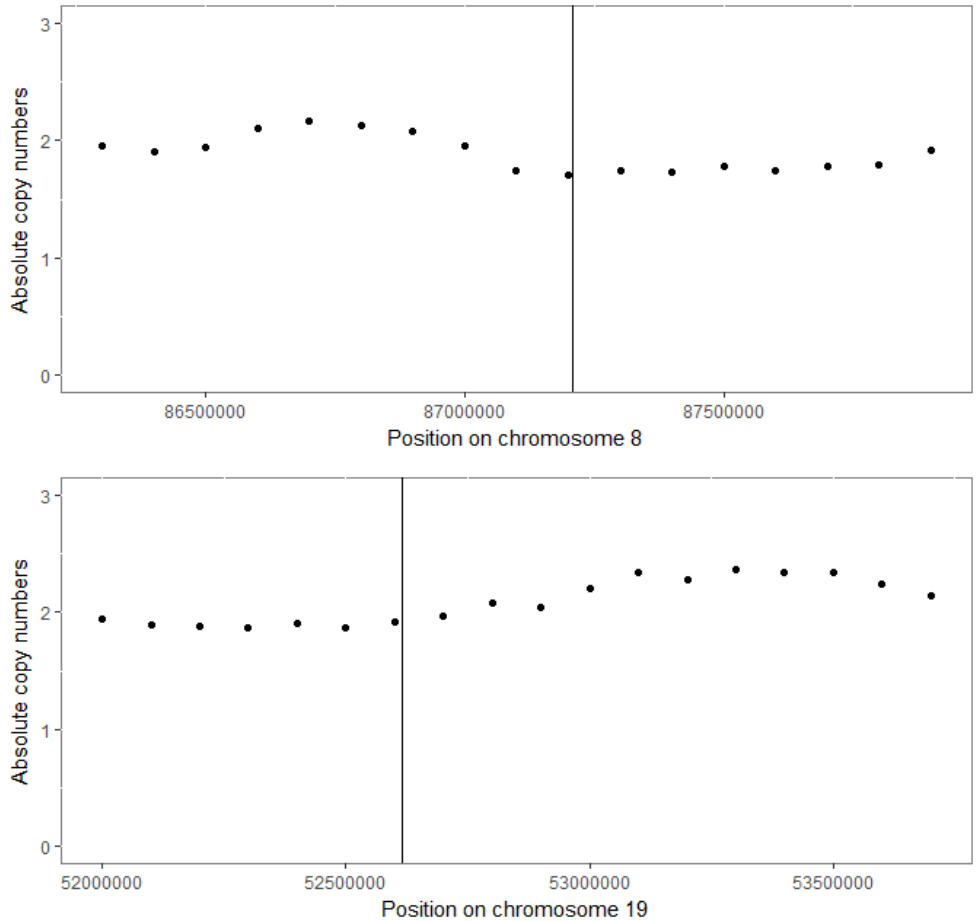

Figure 19. Copy number variations (CNVs) plots across the breakpoint of balanced translocation site at chromosome 8 (upper) and 19 (lower) in 2 Gy-irradiated organoid. There is no alteration of copy number for translocated chromosome. Vertical line: breakpoint on chromosome.

Single Nucleotide Variations

The accumulation of somatic point mutations according to IR dose were evaluated by the amount of SNVs and DNVs (Table 2). The total amount of SNVs in irradiated organoids showed no significant correlation with IR dose (squared linear regression coefficient R^2 of 0.016, p value of 0.742) (Fig. 20, left). Pattern of mutational signature from SNVs also showed no remarkable difference between unirradiated control and irradiated samples due to significant amounts of SNVs characterized by T>C and T>G (Fig. 21). The amount of SNVs in clonal ancestor was 895. The amount of SNVs in 0 Gy control sample was 1969. Among them, 937 were newly developed during culture. Additionally, 775 clonal and 257 non-clonal SNVs were transmitted from ancestor.

However, the total amount of DNVs showed linear correlation with IR dose (R^2 of 0.357, p value of 0.089) (Fig. 21, right and Fig. 22). The correlation between the ratio of DNVs/SNVs and IR dose showed more strong statistical significance (R^2 of 0.576, p value of 0.022). Mutational signatures of DNVs for all organoid genomes characterized by CC>TT. The best-matched patterns of mutational signatures for samples were described in Table 3.

Small insertion and deletions (indels)

Small indels (<50 bp) were categorized by location (non-replicative area of genome vs. replicative area) and type (insertion vs. deletion). A total of 77,755 indels was found as germline mutation. Among them, the amount of indels in clonal ancestor was 1484. There was a significant excess of deletion than insertion (6899 vs. 1265), and both the non-replicative and replicative area indels showed same pattern of enrichment. The total numbers of indels did not show linear relationship with IR dose (Table 4). The amount of SNVs in 0 Gy control sample

was 3017. Among them, 1359 were newly developed during culture. Additionally, 1054 clonal and 604 non-clonal indels were transmitted from ancestor.

However, the number of indels located in non-replicative area increased over the IR dose of 2 Gy (Table 4). In case of 4 Gy- and 8 Gy-irradiated samples, indels were found in exon of organoid genomes (Table 7).

Clustered mutations

We defined clustered mutation as locally multiplied mutations within 20 base pairs including SNVs, DNVs, indels and SVs. A total of 15 loci in irradiated clonal organoids were found as clustered mutation sites and 113 somatic point mutations were analyzed (Fig. 23). Mutational signature of clustered mutation was characterized by C>T (30.1%) which was different with that of SNVs.

Table 2. The accumulation of somatic point mutations induced by IR in clonal pancreas organoids

Organoids	SNV*	DNV**	DNV/SNV ratio (%)	DNV characteristics (numbers > 1)
0 Gy #2	937	6	1.28	GT>TC, TC>CT, AG>GA, CC>AA, TC>GA, CC>TT
1 Gy #1	744	8	2.15	AG>GA, TA>AT, GC>AA, AG>TA, GA>TT, TC>AA, GG>AA
2 Gy #1	905	14	3.09	GT>TC, GC>AA, CT>TG, AC>TA, CC>AT, TA>AC, TC>AA, GG>TT, GG>AA, TA>GT, CC>TT, AC>CA, CC>AA, CA>AG
2 Gy #2	1069	10	1.87	GA>TT, CA>AC, GG>AA, TA>CT, TG>GT, TC>AA, CC>AA, TC>AA, CC>TT, CA>AT
4 Gy #1	868	11	2.53	GA>AC, GG>AA, CA>TG, CA>TG, CC>TT, GG>AT, CC>TT, CT>TG, TC>CT, CC>AG, AA>TG
8 Gy #1	633	13	4.11	CC>AA, TT>AA, CT>AG, TA>AC, CT>TG (2), TC>AT, TC>AA, AT>TA, CC>TT (2), GC>TT, TA>AG

*Single Nucleotide Variations, **Double Nucleotide Variations

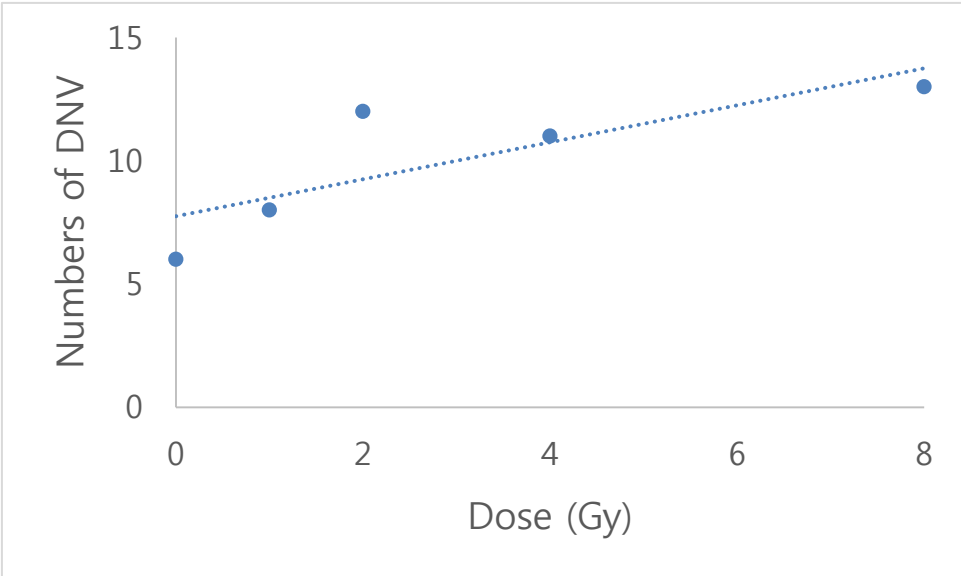

Figure 20. Correlation between IR dose and the amount of double nucleotide variations (DNVs) in clonal pancreas organoids.

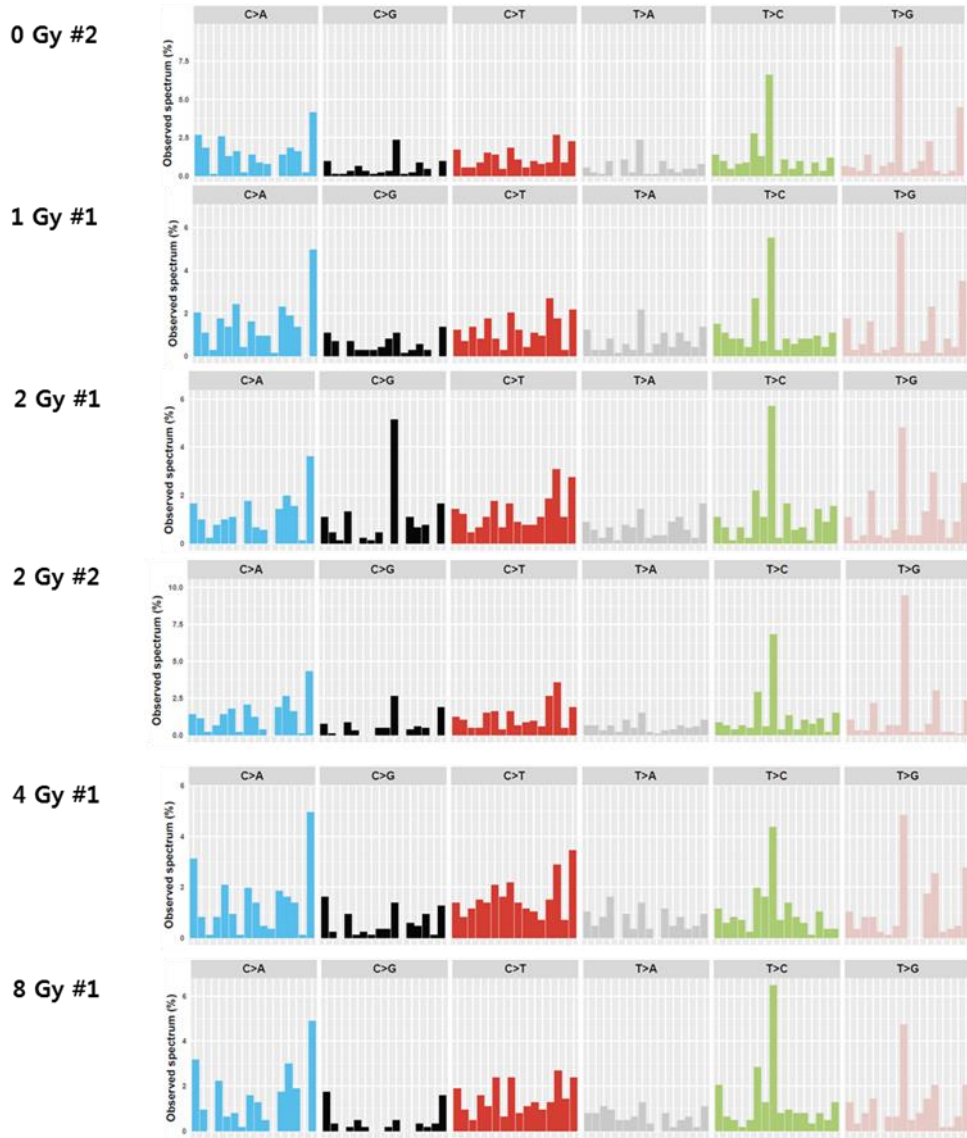

Figure 21. Mutational signatures for SNVs in pancreas samples. In all samples, significant proportion of SNVs were T>C and T>G.

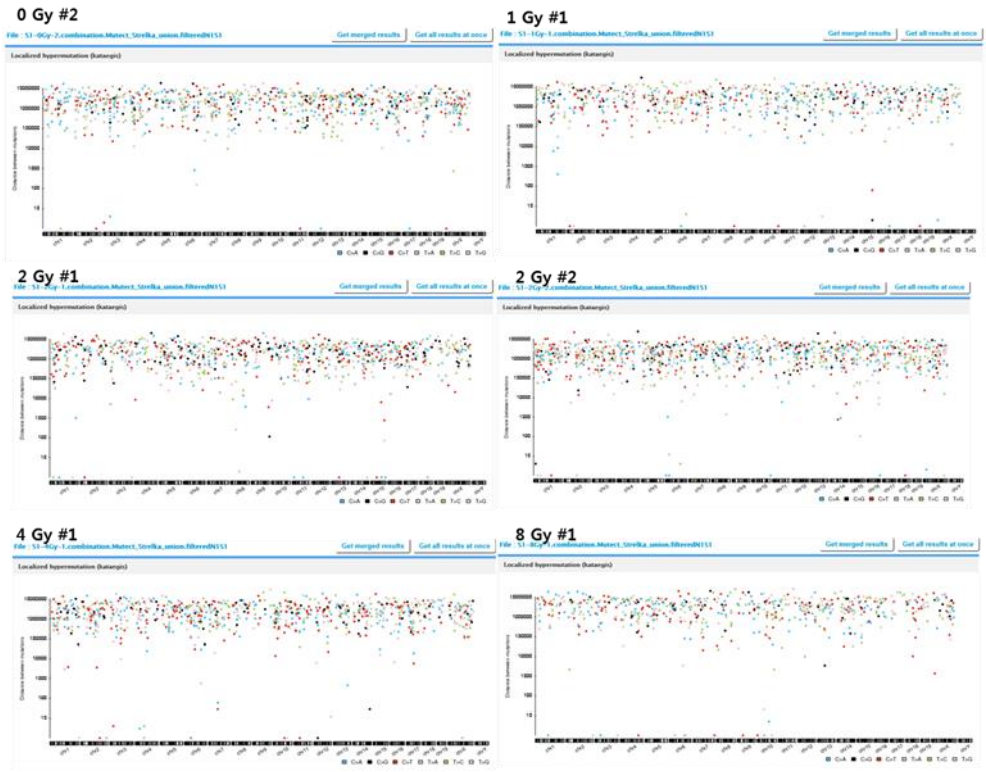

Figure 22. Kataegis plots for visualizing localized hypermutation status of pancreas organoids.

Table 3. The best-matched pattern of mutational signatures for organoid samples

Organoids	Signatures (%)			Cosine Similarity
0 Gy #2	17 (34.5%)	8 (32.7%)	3 (22.3%)	0.947
1 Gy #1	8 (28.9%)	17 (21.0%)	3 (19.8%)	0.942
2 Gy #1	3 (50.3%)	9 (17.9%)	17 (17.7%)	0.888
2 Gy #2	17 (35.3%)	3 (29.0%)	18 (13.4%)	0.947
4 Gy #1	3 (28.0%)	8 (19.2%)	17 (18.3%)	0.945
8 Gy #1	8 (34.3%)	3 (27.7%)	17 (21.2%)	0.914
***Proposed aetiology for signatures (ref. 40)**				
17	Unknown			
8	Unknown			
3	Failure of DNA double-strand break-repair by homologous recombination. Signature 3 is strongly associated with germline and somatic BRCA1 and BRCA2 mutations.			
9	Pattern of mutations that has been attributed to polymerase η, which is implicated with the activity of AID during somatic hypermutation.			
18	Unknown			

Table 4. The small insertion and deletions (Indels) in clonal pancreas organoids.

Dose	**Number of Indels**			
	Location			
	Replicative area		Non-replicative area	
	Insertion	Deletion	Insertion	Deletion
0 Gy	216	1103	4	36
1 Gy	193	1112	4	31
2 Gy	198	1136.5	3.5	55
4 Gy	229	1125	8	62
8 Gy	205	988	3	59

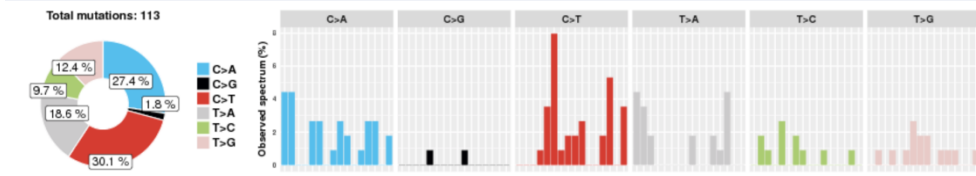

Figure 23. Mutational signatures for clustered somatic point mutations (N = 113).

Part IV. Temporal change of organoid transcriptome after radiation exposure

Firstly, we checked whether the transcription pattern was changed after radiation exposure according to time course. On principal component analysis, there was notable difference of transcription pattern after 2 h of 2 Gy-irradiation (Fig. 24 and 29). Interestingly, there was no remarkable difference of total RNA expression at 30 min after irradiation. The change of RNA expression showed gradual stabilization according to time course (Fig. 24). As well as overexpression of IR-inducible genes, comparable amount of transcriptional repression induced by IR was noted in transcriptomes of 2 h, 6 h, 24 h samples (Fig. 25).

The expression of IR-responsible genes which involve DNA repair mechanism increased at 2 h after irradiation (Fig. 26 a, b). Among them, ATM pathway gene RPA2 (replication protein A2) also increased which was IR-inducible repair pathway. LIG1 (DNA ligase 1) involving alternative NHEJ repair pathway and EXO1 (exonuclease 1) involving mismatch repair also increased which was IR-responsible DNA damage repair pathway (Fig. 26 c, d). TP53 and related gene MDM2 also showed increased expression (Fig. 26 e, f). Other IR-responsible genes such as CDKN1A (cyclin-dependent kinase inhibitor 1a) which functions as a regulator of cell cycle progression at G1 and BTG2 were also increased after 2 h of irradiation (Fig 26 g, h).

Unbiased exploration of gene expression change was performed using unsupervised clustering of irradiated samples genome based on genes with highly variable expression level. In 50 most highly variable genes, 24 showed statistical significance (adjusted p value < 0.001), discernible change of expression level (>1.9 fold change) and functions with possibly related to irradiation responsibility (Table 5). Among them, transcriptional repression (n = 14) was more frequent than

that with transcriptional activation (n = 10). Gene involving apoptotic signaling (MT1X, BIRC5), DNA repair mechanism (PCLAF), cell cycle (MCM5, CCNA2, SHCBP1, CCNB1) and oncogenic process (IQGAP, PBK) showed increased expression after 2 Gy of irradiation. On the other hand, genes involving tumor progression (MUC4, PGF), oxidative scavenger (S100A8, S100A9), cell cycle regulation (SERPINE1, ID3), tumor suppression (DMBT1, DLC1), various molecular (VSIR for NF-kb signaling, DIRAS2 for RAS signaling) and oncogenic (C15orf48, KBTBD11, AGR2) pathways showed decreased expression.

Integrative approach for IR-responsible cellular mechanism was investigated using molecular pathway analysis (Fig 28). Hallmark for DNA repair pathway was enriched in 2 Gy-irradiated organoid transcriptomes (normalized enrichment score NES 1.41, nominal P value 0.005, FDR q value 0.060). Interestingly, hallmark for MYC-targeting pathway was also enriched in 2 Gy-irradiated organoid transcriptomes (NES 2.08, nominal P value <0.001, FDR q value < 0.001).

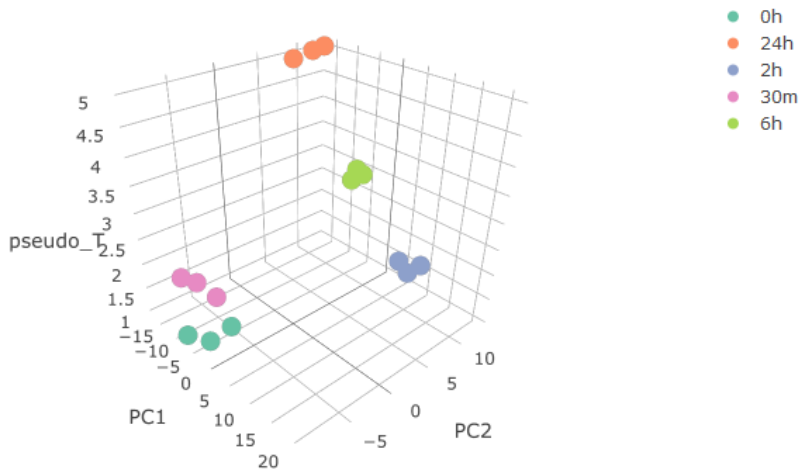

Figure 24. Temporal change of transcription pattern in irradiated pancreas organoids. X axis: first principal component, Y axis: second principal component. Z axis: pseudotime after irradiation.

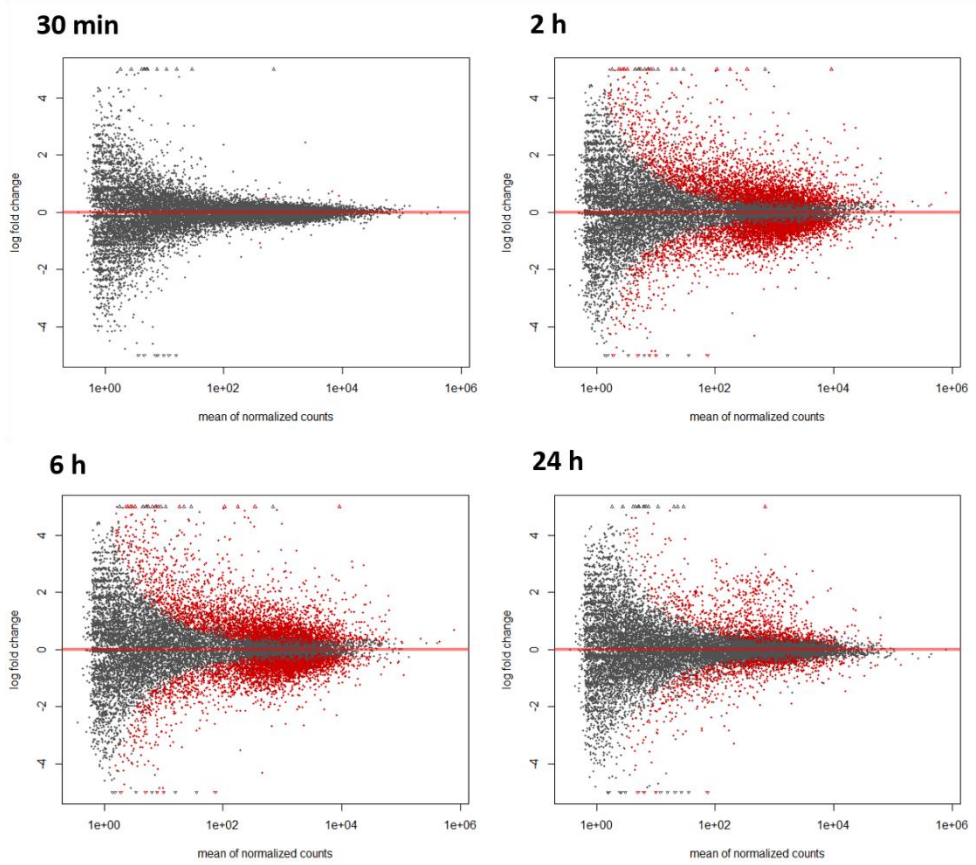

Figure 25. Differential expression of transcripomes according to time course (red dot: adjusted p value < 0.1).

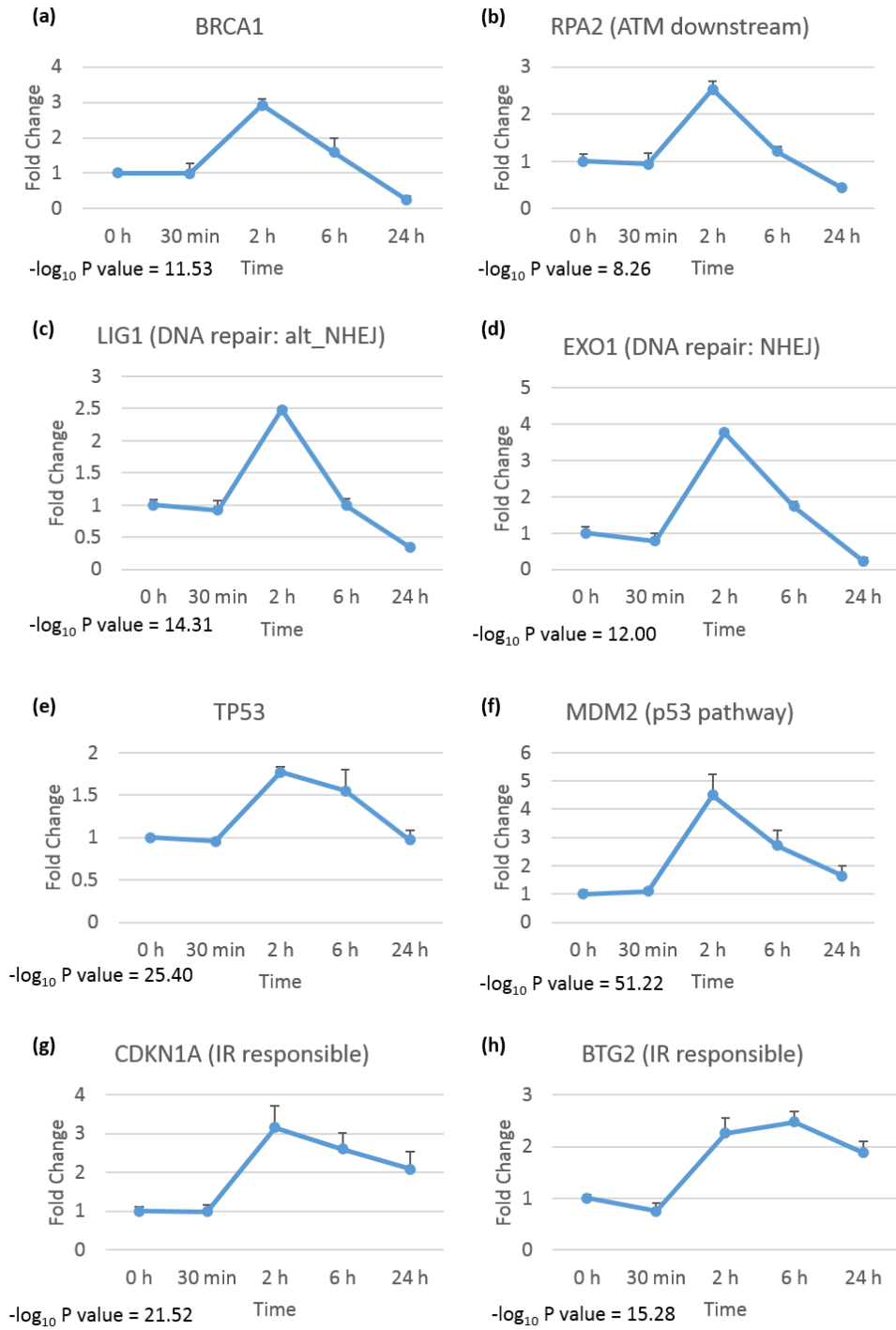

Figure 26. Temporal change of IR-responsible significant gene sets.

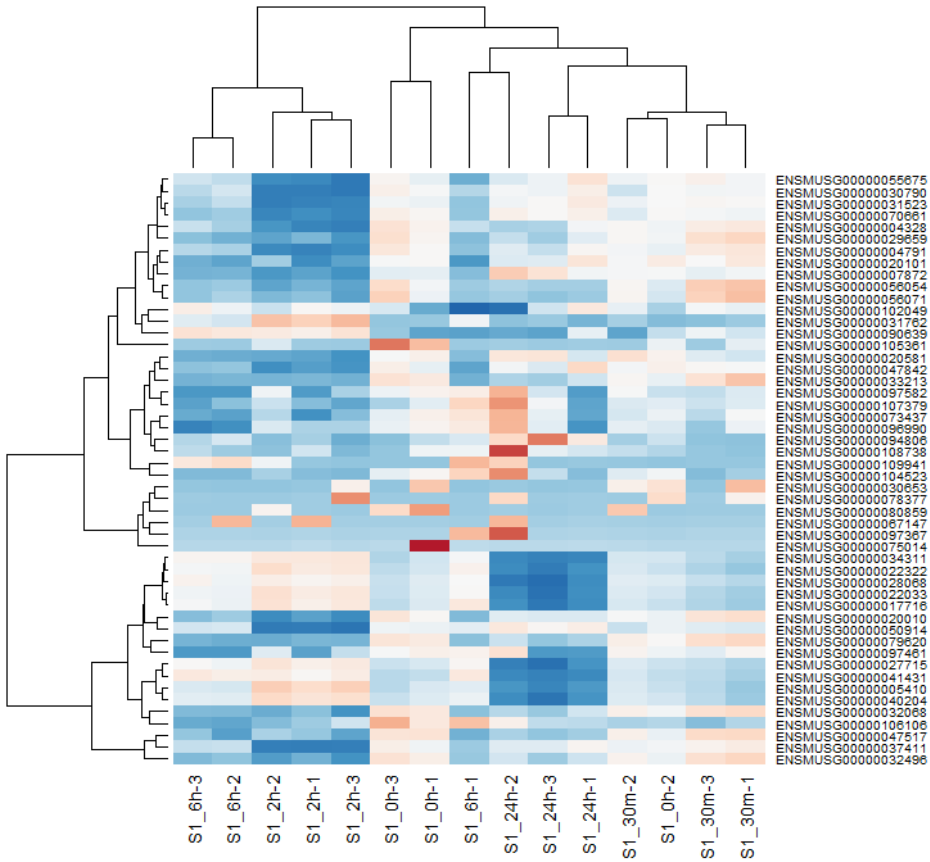

Figure 27. Unsupervised clustering of irradiated sample genomes based on most highly variable 50 genes.

Transcriptional activation		Transcriptional repression	
Genes	**Function**	**Genes**	**Function**
MT1X	Metal binding protein, may be involve anti-apoptotic signaling	MUC4	Tumor progression
PCLAF	PCNA binding protein (DNA repair)	S100 A8,9	Oxidative scavenger
MCM5	Cell cycle progression (Myc pathway)	SERPINE1	Cellular and replicative senescence
BIRC5	Inhibition of apoptosis (found in cervical carcinosarcoma)	ID3	TGF-ß signaling
IQGAP	RAS signaling	C15orf48	Found in esophageal squamous cell carcinoma
CCNA2	Cell cycle regulation	VSIR	NF-kb signaling, T cell signaling
PBK	Found in hematologic cancer, Ewing sarcoma	DMBT1	Probable tumor suppressor gene
KIF4A	Maintaining chromosome integrity	PGF	Growth factor signaling, ERK signaling
SHCBP1	Cytokinesis completion	KBTBD11	CML-associated protein
CCNB1	Proper control of the G2/M transition	DLC1	Tumor suppressor gene
		HIF3A	Regulator of hypoxia-induced gene expression
		AGR2	P53 inhibitor
		DIRAS2	RAS family

Table 5. Critical genes with highly variable expression after irradiation.

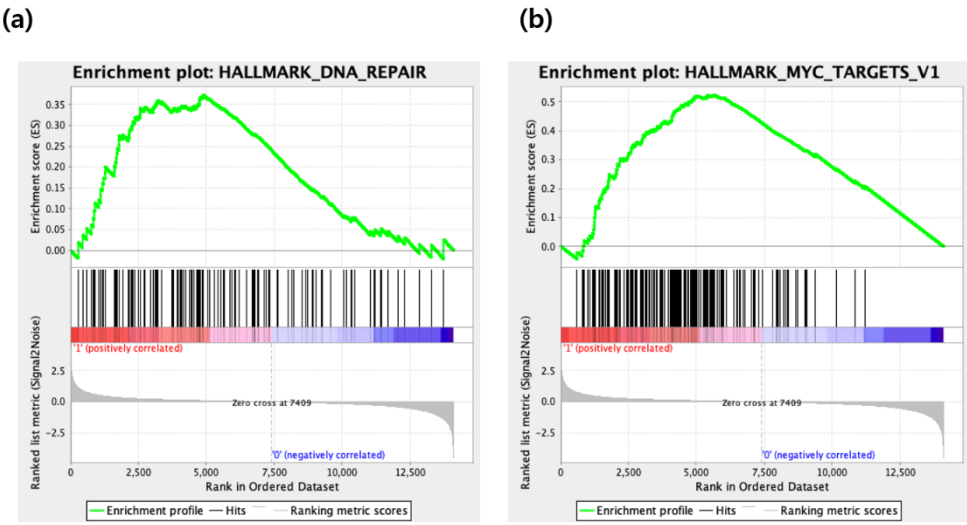

Figure 28. Analysis of IR-induced activating molecular pathway in irradiated pancreas organoids. (a) DNA repair pathway (b) Myc-target pathway.

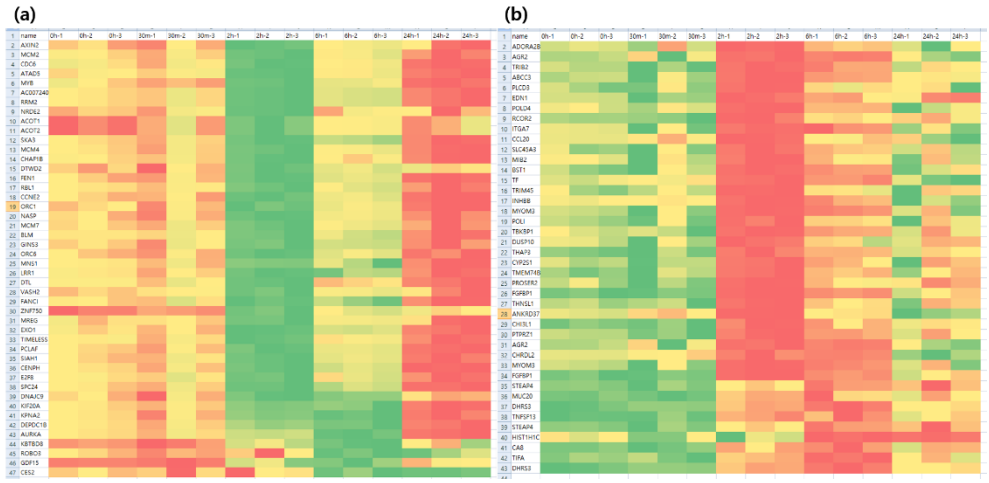

Figure 29. Temporal change of (a) transcriptional activation and (b) transcriptional repression after 2 Gy-irradiation in pancreas organoid. Genes were selected using 2 criteria (-log P value ≥ 4, fold change ≥ 2.5).

Discussion

Recent advances in 3D cell culture technology enable to expand the ASCs outside of the body infinitely. Organoid culture derived from gut ASCs was the first prototype that establish the stem cell niche environment using growth factor cocktails without a mesenchymal niche (22). During the development of organoid culture technology, the critical signaling pathway such as Wnt and Wnt-amplifier including R-spondins has emerged as the key driver of epithelial ASCs-driven organoids (35, 36). Pancreas organoid from isolated ductal ASCs could be cultured long-term under modifying the gut stem cell-culture condition (36). Breast/mammary gland organoid culture is the one that has been studied the latest, and long-term culture protocol has been investigated now. Recently, one study has reported a robust protocol for long-term human mammary epithelial organoid culture (27). We also adapted the reported protocols for pancreas and breast organoid culture, and clonal organoids have been successfully established. One of major strength in study using organoid is its capability for recapitulation and representation of structural and functional properties of organs in vitro easily. Studies for radiation biology could reveal the pathomechanism of organ-specific IR hazard using 3D organoid system.

Lgr5, a receptor for the R-spondins and encoded by a Wnt target gene, marks actively dividing ASCs. Therefore, Lgr5 has been considered as effective target for selecting ASCs in organoid culture (37, 38). Wnt signaling is essential for development of pancreas during embryogenesis (39, 40). In addition, neogenesis of islet after injury in adult pancreas might be derived from Lgr5-positive pancreatic ductal cell which can be enable to establish pancreas organoid (36). Recent study shows that mouse mammary gland organoids can be derived from single Lgr5-positive mammary cells (41). In this study, we establish pancreas and breast organoid from adult mouse primary tissue and confirm the characteristics of organoids by

morphologic phenotype and long-term self-renewal capacity. Previous study reported that the efficiency of clonal organoid establishment after single organoid picking was around 50% (24). The efficiency of clonal organoid establishment was about 91% (10/11) in unirradiated pancreas organoid, but the success rate decreased for breast organoid (~17%, 4/23). This finding might be related to the technical difficulty of breast organoid rupture for expansion. And the efficiency decreased according to IR dose (i.e. only 1 organoid was success in 8 Gy irradiated samples). Further studies under cell sorting using stem cell markers and quantitative analysis for organoid-establishment efficiency will be necessary.

Checking the VAFs of specific heterozygote mutations in DNA isolates might be the most confirmative method for determining clonality of organoid lines. To evaluate the effect of IR for single cell genome, comprehensive filtering process of somatic mutations which was not correlated with radiation exposure is essential. In this study, successful establishment of analysis pipeline for determining clonal organoids can be achieved which is base for analyzing IR-induced somatic mutations using WGS technique.

The survival analysis of irradiated cells has been studied in the *in vitro* setting. For mammalian cells, D_0 dose that induces an average of one lethal event per cell and leaves 37% viable is approximately 1-2 Gy in case of X-ray (7). In this study, survival rate below 50% was shown around the 4 Gy in case of pancreas organoids. The breast organoids showed more radiosensitive feature which of survival was below 50% around the 1 Gy. Breast tissue is one of the most noticeable organ for radiosensitive organ, and the tissue weighting factor for radiation dose was remarkably increased in ICRP 103. Pancreas is the organ that has not received much attention for radiation protection (25). The survival analysis of tissue-specific ASCs after IR exposure might provide critical information for radiation protection of human body. As our knowledge, there is no previous study for evaluating cell

survival curve of irradiated organoids. Nevertheless, the protocol for survival analysis is not optimized in organoids system especially in step of culturing irradiated organoids. Further optimized studies will be necessary for evaluating survival of irradiated organoids *in vitro*.

IR induces senescence of cells leads to an irreversible cell cycle arrest. The activation of the p53 and retinoblastoma (Rb) proteins results in the silencing of genes necessary to promote transition from the G_1 to S phase of the cell cycle. Concomitantly, IR induces cell cycle synchronization due to selective cell killing in radiosensitive phase. Mitosis and the G^2 phase has been known as the most radiosensitive phase, the S phase as most resistant because of HR mechanism (7). However, the proportion of cell cycle in organoids was not significantly changed according to irradiation and/or tissue type in this study. This finding might be related to several factors. First, we analyzed the cell cycle in all cells consisting organoids. Previous study reported that the proportion of Lgr5-highly positive cell population in organoids driven from Lgr5-LacZ knock-in mice is about 1 % (36). Therefore, only small fraction of stem cells and/or progenitor cells in organoids might have dividing capacity. Second, preparation of irradiation experiment itself might be harmful in dissociated single cells from organoids. The proportion of S phase and G_2/M phase is higher in culturing pancreas organoids than in unirradiated control pancreas organoids (S phase: 6.2 vs. 2.9 %, G_2/M phase: 13.2 vs. 4.8 %, respectively) (Fig. 30). Previous *in vitro* studies for cell survival and/or cell cycle analysis in radiation experiments have used immortalized cells or cancer cells which have different physiology from normal cells (42). Further studies resembling physiologic body condition will be necessary for accurate prediction of IR-induced cell cycle arrest.

The impaired DSB repair increases chromosome aberrations in mammalian cells. The types of chromosomal aberrations are either lethal to the cell or non-lethal

but involved in carcinogenesis. The lethal aberrations are the dicentric, ring and anaphase bridges. The non-lethal type of chromosomal aberrations include balanced translocation, balanced inversion and small deletion. Chromosomal aberrations analyzed in peripheral blood lymphocytes have been used as representative biomarkers of IR exposure with dose-dependent manner (7). Balanced inversion has been known as extremely rare type of chromosomal rearrangement arising from genes broken at either end of the inversion, followed head-to-head and tail-to-tail rejoining and could be hallmark of radiation-induced secondary malignancy (43). In this study, balanced inversion was noted in irradiated normal ASCs (Table 6.). Furthermore, no complex SVs such as breakage-fusion-bridge cycles, chromothripsis and chromoplexy were found. From these findings, we suggest that IR induces balanced chromosomal instability which might be specific mutational signatures. Analysis of specific type of IR-induced somatic mutation in normal cells and relationship between IR-induced malignancies might be essential for assessing IR-induced carcinogenesis.

IR-induced small indels has been regarded that a significant excess of deletions relative to insertions (43, 44). These findings are related that NHEJ is the repair mechanism of IR-induced deletion. In this study, deletion is more frequently found than insertion. Additionally, indels in non-replicative genome area showed tendency to dose-relationship. Microhomology-mediated end-joining (MMEJ) can occur in repair of DSB which is not resulted caused by replication slippage. Factors for MMEJ processing is independent of the canonical NHEJ such as DNA-PK, Ku70 and XRCC4. Based on the frequency of microhomology at the breakpoints, NHEJ and MMEJ seemed to involve in the DNA repair with similar ratio in pancreas organoids. And the proportion of NHEJ for DNA repair seemed to be slightly higher in breast organoids (Table 7, Fig. 11). NHEJ have been considered to induce complex genomic rearrangement from a single catastrophic event such as chromothripsis. One

report for studying human cancer genome showed that breast cancer is related to MMEJ more frequently than other tumor types(34). BRCA1-defective cancer are associated with SVs that exhibit a breakpoint footprint of template insertion(45). Further studies for quantitative analysis of IR-induced SVs and repair mechanism might be helpful to evaluate IR-induced carcinogenesis.

Copy number change of chromosomal arm level was only found in 1 case of 2 Gy irradiated organoid. This finding might be due to a small number of samples in this study. Interestingly, unirradiated control organoid (11 passages at DNA isolating time) also shows no chromosomal loss. Recent study reported that epithelial cells have increased chromosome mis-segregation outside of their native tissues (46). Therefore, studying cells *in vitro* should keep maintaining chromosome stability for revealing physiologic *in vivo* cell fate. Organoid culture system might have advantage in view of *in vitro* culture resembling tissue environment for studying IR-induced mutagenesis.

Mutational signatures from somatic substitutions and small indels have been studied for revealing and determining the biologic mechanism of mutational process based on WGS data (47). Although the mutational signatures induced from environmental carcinogens such as smoking and ultraviolet light are suggested (48), there is no comprehensive analysis for mutational signatures from IR until now. In this study, *in vitro* cultured clonal organoids have significant amount of SNVs. Previous report for studying normal mouse organoid showed that mutations acquired *in vitro* characterized by T>G mutations enriched at XpTpT trinucleotides (49). Similarly, both the genome of ancestor and unirradiated control have mutational signatures for T>G. The mutational process induced by *in vitro* culture might be related to this finding. Furthermore, SNVs did not remarkably increase according to IR dose. Mutational signatures from SNVs induced by IR would be studied further.

IR induces somatic mutation along the radiation track structures and the

mechanism of DNA damage is explained by clustered damages. Low linear energy transfer IR such as gamma-rays deposits its energy in the water surrounding the DNA molecules within a cluster of radius 4 nm (50-52). In this study, DNVs increased according to IR dose. And mutational signatures for clustered damage sites was characterized by C>T which differed from SNVs signatures. IR-induced DNA damages consisted of direct damage and reactive free radicals produced by radiolysis. DNA damages by oxidants could be induced during normal oxidative metabolism which present at significant amount regardless of IR (53, 54). Therefore, analysis of IR-specific mutational signature might be essential to assess the accurate mechanism of IR-induced carcinogenesis in human body.

Several studies have reported the RNA-based gene expression profile of radiation induced molecular pathways. Study for irradiation of tumorigenic human epithelial cells showed that tissue-specific gene tended to be transcriptional repression while more house-keeping genes showed activated when comparing with the immortalized tissue specific mammary epithelial cells (55). The relationship between DNA damage from IR and apoptosis progression was not fully revealed yet. One study showed that micronuclei resulting from IR induced DNA damage correlated with RNA expression pattern to assess radiation sensitivity, but BAX/BCL2 didn't show positive correlation (56). In our study, gene expression profile showed tendency to inhibit apoptosis (negatively enriched genes: BCL2L1/L2, CDKN1B, MGMT, CASP1, etc). It might be related to the protective mechanism of sublethal damage from IR. Study for using germline BRCA1 mutation carrier showed that BRCA1 mutation carrier had a distinctive gene expression phenotype after IR induced DNA damage(57). The significant gene set correlated to BRCA1 include CDKN1B, ATR and RAD51. Our result showed similar pattern of increased BRCA1 expression combined with CDKN1B down-regulation. BRCA1 have been known as the risk factor of pancreatic cancer (relative risk 2.26), as well

as the standardized incidence ratio for pancreatic cancer was about 2.55 (58). The IR-induced activation of BRCA1 and related molecular pathway might be the cause of carcinogenesis in pancreas. Metallothioneins are modulators of metal toxicity and important mediators of oxidative damage with a specific role in radical scavenging after radiation exposure (59). Concordantly, MT1X gene was one of the most significant genes after IR in our study (log2 fold change 4.32, adjusted p value 3.14E-57). Inflammatory and immunity processes have been considered as critical response in bystander cells after irradiation (60). On the contrary, our result based on irradiated organoids showed negative enrichment of hallmark for inflammatory response (NES -1.38, nominal p value 0.024, FDR q value 0.107) as well as VSIR gene repression. Further study designed by discriminating IR response in irradiated organoids and bystander might be useful for evaluating bystander effect. ERK1/2 activation has been considered as key step for IR-induced G2/M phase arrest (61). Although the lack of molecular data for phosphorylation profile of ERK proteins, increased expression of CDC25A (fold change 1.60, adjust p value 0.0002) in 2 h samples might be the consequence of 2 Gy irradiation in our experiment. Induction of CDKN1A and MDM2 is the most consistent marker for IR exposure (62, 63). Also in our study, CDKN1A and MDM2 expression was highly increased after 2 h of irradiation (fold change 2.99, adjusted p value 3.04E-22; fold change 4.23, adjusted p value 5.98E-52, respectively). The proto-oncogene c-myc has been regarded as a central switch in the onset or progression of many types of cancer. The effects of c-myc overexpression might contribute to genomic instability which might be related to IR induced carcinogenesis (64). Overexpression of c-Myc attenuated G1/S arrest following IR and induced the inappropriate DNA synthesis. IR experiment using c-Myc overexpressed breast cancer cell line showed the inappropriate hyperphosphorylation of Rb and reappearance of cyclin A. In our study, enrichment of Myc-target pathway is one of the key finding in pathway analysis. The role of

Myc in IR-induced carcinogenesis need to be further investigated. Previous study using irradiated mouse blood showed the bidirectional change of expression level in E2F2(65). This gene was consistently downregulated at D1 post-irradiation and upregulated in D7 which was different expression pattern with other E2F genes. Target genes of E2F include hundreds of genes and not fully understood in IR responsibility. In our study, hallmark for E2F targets pathway was remarkably enriched (NES 2.74, nominal p value <0.001, FDR q value <0.001). Further integrative study for evaluating the role of E2F signaling in irradiated organoid might be needed. Radiation-derived gene expression signatures can predict clinical outcome for breast cancer(66). Interestingly, DNA polymerase POLH didn't show increased expression after irradiation which was considered to be UV-induced damage repair pathway. On the contrary, DNA polymerase POLQ showed increased expression (log2 fold change 1.025, Adj. P value 8.49E-5) after 2 h of irradiation which was considered to be IR-induced damage repair pathway(67). Studying for gene expression profile in radiation research would be necessary not only for investigating molecular mechanism of IR-induced cellular response but for predicting the prognosis of irradiated patient.

Study for evaluating the effect of IR on the proliferation of human embryonic stem cells showed that remarkable difference presented in doubling time and relative cell survival between individual colonies from the cell line(68). The researchers explained that colony organization is base for maintaining "stemness" of stem cells and p53-based molecular pathway could involve colony proliferation, preventing differentiation and controlling cell competitions(69). Further studies need to investigate the role of p53-based molecular pathway in stem cells with radiation biology context.

Several limitation is present in our study. First, relative small number of single cell genomes were analyzed although the sample-size estimate was not

calculated. Second, molecular evidence of protein-level change according to IR was not included. Lastly, integrative approach between IR-induced mutational signatures and consequence of transriptome changes was not fully adopted. Future studies including various tissue-specific ASCs might be helpful for IR response of human body with in vivo irradiation context. IR-specific mutational signatures during imprecise repair of ASC genome would be further investigated. Finally, key regulator genes for cellular response after IR need to be clarified for studying IR-induced carcinogenesis.

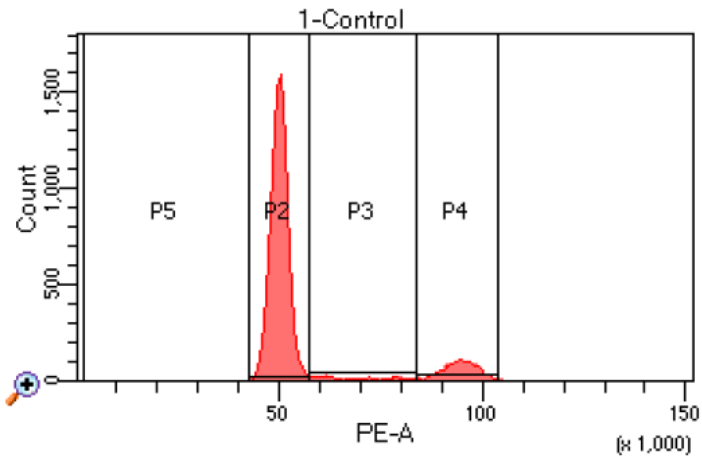

Figure 30. Histogram plots of cell cycle analysis for culturing pancreas organoids. The cells were stained with propidium iodide (PI). Fluorescence activated cell sorting (FACS) analysis was performed for chromosome content measurement.

Table 6. Inversions found in clonal pancreas organoids.

Organoids	**Chr**	**Head to Head inversion**		**Tail to tail inversion**		**Breakpoint at**		**Size (bp)**
		>>Ascending coordinates	<< Inverted segment <<		>>Ascending coordinates	Head to head inversion	Tail to tail inversion	
		5’ coordinate	3’ coordinate	5’ coordinate	3’ coordinate	Microhomology	Microhomology	
2 Gy #2	3	76573451	79420189	79421619	79420621	-	T	430
2 Gy #2	11	20105104	20105105	20176077	20176089	GT	-	70972
4 Gy #1	16	54349661	54349672	77138836	77138846	GA	G	22,789,164
8 Gy #1	14	70359032	70359033	108819678	108819679	-	-	38,460,646
	14	70359032	70359051	108819678	108819679	-	-	38,460,627

Table 7. Indels found in exon of pancreas organoid genomes

Organoids	Chr	Position	Wildtype Sequence	Mutant Sequence	Gene
4 Gy #1	5	123015386	-	CCGCTG	ORAI1
	13	95364725	CTGTCTCCATCATAGCTCTTCTCACTCTGAGAGT	-	AGGF1
8 Gy #1	2	82257358	-	A	ZFP804A
	7	4028917	C	-	LAIR1
	18	25496187	TTCAGGGAGCGGGGAAGGGAGGGGCAGAGACTCACCT	-	CELF4

Conclusion

3D Organoid cultures for tissue-specific ASCs were adapted for studying gamma radiation-induced somatic mutations. The survival analysis after irradiation of organoids revealed that cells from pancreas and breast showed different survival rates which might reflect tissue-specific radiation sensitivity. The pipeline for analyzing IR-induced somatic mutations in WGS context was constructed. IR-related chromosomal SVs including deletion, balanced inversion, translocation and complex SVs were found in irradiated organoid genome with dose-dependent manner which implicated the markers for IR-induced genomic damages. IR-induced clustered DNA damages such as DNVs could be represented as mutational signatures by IR. Further studies for analyzing IR-induced somatic mutation could reveal the mechanism of radiation-induced carcinogenesis in human body.

References

1. Muller HJ. Artificial Transmutation of the Gene. Science. 1927;66(1699):84-7.

2. Shigematsu I, Kagan A. Cancer in atomic bomb survivors. Tokyo
New York: Japan Scientific Societies Press ;
Plenum Press; 1986. vi, 196 p. p.

3. Leuraud K, Richardson DB, Cardis E, Daniels RD, Gillies M, O'Hagan JA, et al. Ionising radiation and risk of death from leukaemia and lymphoma in radiation-monitored workers (INWORKS): an international cohort study. Lancet Haematol. 2015;2(7):e276-81.

4. Folley JH, Borges W, Yamawaki T. Incidence of leukemia in survivors of the atomic bomb in Hiroshima and Nagasaki, Japan. Am J Med. 1952;13(3):311-21.

5. Preston DL, Shimizu Y, Pierce DA, Suyama A, Mabuchi K. Studies of mortality of atomic bomb survivors. Report 13: Solid cancer and noncancer disease mortality: 1950-1997. Radiat Res. 2003;160(4):381-407.

6. Richardson D, Sugiyama H, Nishi N, Sakata R, Shimizu Y, Grant EJ, et al. Ionizing radiation and leukemia mortality among Japanese Atomic Bomb Survivors, 1950-2000. Radiat Res. 2009;172(3):368-82.

7. Hall EJ, Giaccia AJ. Radiobiology for the radiologist. 6th ed. Philadelphia: Lippincott Williams & Wilkins; 2006. ix, 546 p. p.

8. Lengauer C, Kinzler KW, Vogelstein B. Genetic instabilities in human cancers. Nature. 1998;396(6712):643-9.

9. Sutherland BM, Bennett PV, Sutherland JC, Laval J. Clustered DNA damages induced by x rays in human cells. Radiat Res. 2002;157(6):611-6.

10. Ward JF. DNA damage produced by ionizing radiation in mammalian cells: identities, mechanisms of formation, and reparability. Prog Nucleic Acid Res Mol

Biol. 1988;35:95-125.

11. Blyth BJ, Kakinuma S, Sunaoshi M, Amasaki Y, Hirano-Sakairi S, Ogawa K, et al. Genetic Analysis of T Cell Lymphomas in Carbon Ion-Irradiated Mice Reveals Frequent Interstitial Chromosome Deletions: Implications for Second Cancer Induction in Normal Tissues during Carbon Ion Radiotherapy. PLoS One. 2015;10(6):e0130666.

12. Nieri D, Berardinelli F, Antoccia A, Tanzarella C, Sgura A. Comparison between two FISH techniques in the in vitro study of cytogenetic markers for low-dose X-ray exposure in human primary fibroblasts. Frontiers in Genetics. 2013;4:141.

13. Russell WL, Kelly EM. Mutation frequencies in male mice and the estimation of genetic hazards of radiation in men. Proc Natl Acad Sci U S A. 1982;79(2):542-4.

14. Tounekti O, Kenani A, Foray N, Orlowski S, Mir LM. The ratio of single- to double-strand DNA breaks and their absolute values determine cell death pathway. British Journal Of Cancer. 2001;84:1272.

15. Willers H, Dahm-Daphi J, Powell SN. Repair of radiation damage to DNA. Br J Cancer. 2004;90(7):1297-301.

16. Sage E, Shikazono N. Radiation-induced clustered DNA lesions: Repair and mutagenesis. Free Radical Biology and Medicine. 2017;107:125-35.

17. Stratton MR, Campbell PJ, Futreal PA. The cancer genome. Nature. 2009;458(7239):719-24.

18. Barker N, Ridgway RA, van Es JH, van de Wetering M, Begthel H, van den Born M, et al. Crypt stem cells as the cells-of-origin of intestinal cancer. Nature. 2009;457(7229):608-11.

19. Milholland B, Auton A, Suh Y, Vijg J. Age-related somatic mutations in the cancer genome. Oncotarget. 2015;6(28):24627-35.

20. Tomasetti C, Vogelstein B. Cancer etiology. Variation in cancer risk among

tissues can be explained by the number of stem cell divisions. Science. 2015;347(6217):78-81.

21. Blokzijl F, de Ligt J, Jager M, Sasselli V, Roerink S, Sasaki N, et al. Tissue-specific mutation accumulation in human adult stem cells during life. Nature. 2016;538(7624):260-4.

22. Sato T, Vries RG, Snippert HJ, van de Wetering M, Barker N, Stange DE, et al. Single Lgr5 stem cells build crypt-villus structures in vitro without a mesenchymal niche. Nature. 2009;459(7244):262-5.

23. Clevers H. Modeling Development and Disease with Organoids. Cell. 2016;165(7):1586-97.

24. Jager M, Blokzijl F, Sasselli V, Boymans S, Janssen R, Besselink N, et al. Measuring mutation accumulation in single human adult stem cells by whole-genome sequencing of organoid cultures. Nat Protoc. 2018;13(1):59-78.

25. The 2007 Recommendations of the International Commission on Radiological Protection. ICRP publication 103. Ann ICRP. 2007;37(2-4):1-332.

26. Broutier L, Andersson-Rolf A, Hindley CJ, Boj SF, Clevers H, Koo BK, et al. Culture and establishment of self-renewing human and mouse adult liver and pancreas 3D organoids and their genetic manipulation. Nat Protoc. 2016;11(9):1724-43.

27. Sachs N, de Ligt J, Kopper O, Gogola E, Bounova G, Weeber F, et al. A Living Biobank of Breast Cancer Organoids Captures Disease Heterogeneity. Cell. 2018;172(1-2):373-86 e10.

28. Li H, Durbin R. Fast and accurate short read alignment with Burrows-Wheeler transform. Bioinformatics. 2009;25(14):1754-60.

29. Cibulskis K, Lawrence MS, Carter SL, Sivachenko A, Jaffe D, Sougnez C, et al. Sensitive detection of somatic point mutations in impure and heterogeneous cancer samples. Nat Biotechnol. 2013;31(3):213-9.

30. Koboldt DC, Zhang Q, Larson DE, Shen D, McLellan MD, Lin L, et al. VarScan 2: somatic mutation and copy number alteration discovery in cancer by exome sequencing. Genome Res. 2012;22(3):568-76.

31. Sherry ST, Ward MH, Kholodov M, Baker J, Phan L, Smigielski EM, et al. dbSNP: the NCBI database of genetic variation. Nucleic Acids Res. 2001;29(1):308-11.

32. Lee J, Lee AJ, Lee JK, Park J, Kwon Y, Park S, et al. Mutalisk: a web-based somatic MUTation AnaLyIS toolKit for genomic, transcriptional and epigenomic signatures. Nucleic Acids Res. 2018;46(W1):W102-W8.

33. Love MI, Huber W, Anders S. Moderated estimation of fold change and dispersion for RNA-seq data with DESeq2. Genome Biol. 2014;15(12):550.

34. Yang L, Luquette LJ, Gehlenborg N, Xi R, Haseley PS, Hsieh CH, et al. Diverse mechanisms of somatic structural variations in human cancer genomes. Cell. 2013;153(4):919-29.

35. Clevers H, Loh KM, Nusse R. Stem cell signaling. An integral program for tissue renewal and regeneration: Wnt signaling and stem cell control. Science. 2014;346(6205):1248012.

36. Huch M, Bonfanti P, Boj SF, Sato T, Loomans CJ, van de Wetering M, et al. Unlimited in vitro expansion of adult bi-potent pancreas progenitors through the Lgr5/R-spondin axis. EMBO J. 2013;32(20):2708-21.

37. Barker N, Huch M, Kujala P, van de Wetering M, Snippert HJ, van Es JH, et al. Lgr5(+ve) stem cells drive self-renewal in the stomach and build long-lived gastric units in vitro. Cell Stem Cell. 2010;6(1):25-36.

38. Barker N, van Es JH, Kuipers J, Kujala P, van den Born M, Cozijnsen M, et al. Identification of stem cells in small intestine and colon by marker gene Lgr5. Nature. 2007;449(7165):1003-7.

39. Heiser PW, Lau J, Taketo MM, Herrera PL, Hebrok M. Stabilization of

beta-catenin impacts pancreas growth. Development. 2006;133(10):2023-32.

40. Murtaugh LC, Law AC, Dor Y, Melton DA. Beta-catenin is essential for pancreatic acinar but not islet development. Development. 2005;132(21):4663-74.

41. Zhang L, Adileh M, Martin ML, Klingler S, White J, Ma X, et al. Establishing estrogen-responsive mouse mammary organoids from single Lgr5(+) cells. Cell Signal. 2017;29:41-51.

42. Steel GG. From targets to genes: a brief history of radiosensitivity. Physics in medicine and biology. 1996;41(2):205-22.

43. Behjati S, Gundem G, Wedge DC, Roberts ND, Tarpey PS, Cooke SL, et al. Mutational signatures of ionizing radiation in second malignancies. Nat Commun. 2016;7:12605.

44. Okudaira N, Uehara Y, Fujikawa K, Kagawa N, Ootsuyama A, Norimura T, et al. Radiation dose-rate effect on mutation induction in spleen and liver of gpt delta mice. Radiation research. 2010;173(2):138-47.

45. Waszak SM, Tiao G, Zhu B, Rausch T, Muyas F, Rodriguez-Martin B, et al. Germline determinants of the somatic mutation landscape in 2,642 cancer genomes. bioRxiv. 2017:208330.

46. Knouse KA, Lopez KE, Bachofner M, Amon A. Chromosome Segregation Fidelity in Epithelia Requires Tissue Architecture. Cell. 2018;175(1):200-11 e13.

47. Alexandrov LB, Nik-Zainal S, Wedge DC, Aparicio SA, Behjati S, Biankin AV, et al. Signatures of mutational processes in human cancer. Nature. 2013;500(7463):415-21.

48. Pfeifer GP. Environmental exposures and mutational patterns of cancer genomes. Genome Med. 2010;2(8):54.

49. Behjati S, Huch M, van Boxtel R, Karthaus W, Wedge DC, Tamuri AU, et al. Genome sequencing of normal cells reveals developmental lineages and mutational processes. Nature. 2014;513(7518):422-5.

50. Brenner DJ, Ward JF. Constraints on energy deposition and target size of multiply damaged sites associated with DNA double-strand breaks. Int J Radiat Biol. 1992;61(6):737-48.

51. Goodhead DT. Initial events in the cellular effects of ionizing radiations: clustered damage in DNA. Int J Radiat Biol. 1994;65(1):7-17.

52. Nikjoo H, O'Neill P, Terrissol M, Goodhead DT. Modelling of radiation-induced DNA damage: the early physical and chemical event. Int J Radiat Biol. 1994;66(5):453-7.

53. Beckman KB, Ames BN. Oxidative decay of DNA. J Biol Chem. 1997;272(32):19633-6.

54. Henle ES, Linn S. Formation, prevention, and repair of DNA damage by iron/hydrogen peroxide. J Biol Chem. 1997;272(31):19095-8.

55. Ma L, Nie L, Liu J, Zhang B, Song S, Sun M, et al. An RNA-seq-based gene expression profiling of radiation-induced tumorigenic mammary epithelial cells. Genomics Proteomics Bioinformatics. 2012;10(6):326-35.

56. Bishay K, Ory K, Olivier MF, Lebeau J, Levalois C, Chevillard S. DNA damage-related RNA expression to assess individual sensitivity to ionizing radiation. Carcinogenesis. 2001;22(8):1179-83.

57. Kote-Jarai Z, Williams RD, Cattini N, Copeland M, Giddings I, Wooster R, et al. Gene expression profiling after radiation-induced DNA damage is strongly predictive of BRCA1 mutation carrier status. Clin Cancer Res. 2004;10(3):958-63.

58. Iqbal J, Ragone A, Lubinski J, Lynch HT, Moller P, Ghadirian P, et al. The incidence of pancreatic cancer in BRCA1 and BRCA2 mutation carriers. Br J Cancer. 2012;107(12):2005-9.

59. Laukens D, Waeytens A, De Bleser P, Cuvelier C, De Vos M. Human metallothionein expression under normal and pathological conditions: mechanisms of gene regulation based on in silico promoter analysis. Crit Rev Eukaryot Gene Expr.

2009;19(4):301-17.

60. Ghandhi SA, Sinha A, Markatou M, Amundson SA. Time-series clustering of gene expression in irradiated and bystander fibroblasts: an application of FBPA clustering. BMC Genomics. 2011;12:2.

61. Yan Y, Black CP, Cowan KH. Irradiation-induced G2/M checkpoint response requires ERK1/2 activation. Oncogene. 2007;26(32):4689-98.

62. Snyder AR, Morgan WF. Gene expression profiling after irradiation: clues to understanding acute and persistent responses? Cancer Metastasis Rev. 2004;23(3-4):259-68.

63. Perry ME. Mdm2 in the response to radiation. Mol Cancer Res. 2004;2(1):9-19.

64. Sheen JH, Dickson RB. Overexpression of c-Myc alters G(1)/S arrest following ionizing radiation. Mol Cell Biol. 2002;22(6):1819-33.

65. Broustas CG, Xu Y, Harken AD, Garty G, Amundson SA. Comparison of gene expression response to neutron and x-ray irradiation using mouse blood. BMC Genomics. 2017;18(1):2.

66. Piening BD, Wang P, Subramanian A, Paulovich AG. A radiation-derived gene expression signature predicts clinical outcome for breast cancer patients. Radiat Res. 2009;171(2):141-54.

67. Lange SS, Takata K, Wood RD. DNA polymerases and cancer. Nat Rev Cancer. 2011;11(2):96-110.

68. Panyutin IV, Holar SA, Neumann RD, Panyutin IG. Effect of ionizing radiation on the proliferation of human embryonic stem cells. Sci Rep. 2017;7:43995.

69. Dejosez M, Ura H, Brandt VL, Zwaka TP. Safeguards for cell cooperation in mouse embryogenesis shown by genome-wide cheater screen. Science. 2013;341(6153):1511-4.

국 문 초 록

방사선에 의해 유도된 정상 오가노이드 내 체성돌연변이에 대한 전장유전체 분석

권현우
서울대학교
융합과학기술대학원
분자의학 및 바이오제약학과

목적:
본 연구진은 전리방사선 중 하나인 감마선이 유발하는 성체줄기세포 내 체성돌연변이의 패턴 및 방사선량과의 관련성을 평가하는 연구를 수행하였다. 조직특이적 성체줄기세포를 오가노이드 배양기술을 적용하여 실험실내 배양을 수행하였고, 전리방사선 피폭 후 유발된 체성돌연변이의 정량적 평가를 위해 배양된 오가노이드의 전장유전체 분석을 수행하였다.

방법:
정상 C57BL/6 암컷 쥐의 췌장과 유선조직에서 성체줄기세포를 분리하여 알려진 조직특이적 성장인자들의 조합을 이용한 실험실내 오가노이드 배양을 수행하였고 단일 오가노이드의 선택적 배양을 통해 클론 오가노이드를 확립하였다. 배양된 오가노이드를 단일세포로 분리 후 감마선 조사기를 이용하여 1-10 Gy 의 감마선을 오가노이드에

조사하였다. 방사선 피폭에 따른 오가노이드의 생존분석을 수행하였다. 방사선 조사 후 오가노이드를 형광 유세포 계측기술을 이용하여 단일세포로 분리하고 재배양하였다. 방사선 피폭 후 생존한 클론 오가노이드의 DNA를 추출하여 30X 범위 전장유전체서열분석을 수행하였다. 얻어진 염기서열을 토대로 방사선에 의해 유발된 체성돌연변이를 각각 염색체 결실, 염색체 구조이상, 단일염기서열변이, 이중염기서열 변이, 군집돌연변이로 분류하고 이의 정량적, 정성적 분석을 수행하였다. 방사선이 미치는 오가노이드 내 신호전달 체계의 변화를 확인하기 위해 2 Gy의 감마선을 췌장 오가노이드에 조사 후 시간의 흐름에 따라 (0 h, 30 min, 2 h, 6 h, 24 h) 오가노이드 내 전체 RNA를 수집하였다. 방사선에 반응하는 중요한 유전자들의 발현 차이 여부를 통해 방사선 특이 유전자들을 확인하였고 이를 바탕으로 방사선에 의해 활성화된 분자 기전을 탐색하였다.

결과:

정상 쥐에서 유래한 췌장, 유선 오가노이드의 배양 및 클론 오가노이드의 확립을 성공하였고 개별 오가노이드에 특이적인 단일염기서열 변이를 이용하여 클론 오가노이드 여부를 확인하였다. 유선 오가노이드 (1 Gy 전후에서 50% 생존 확인)는 췌장 오가노이드 (4 Gy 전후에서 50% 생존 확인)에 비해 좀더 방사선에 민감한 경향을 보였다. 6개의 췌장 오가노이드 전장유전체 분석 결과 1개의 2 Gy 피폭을 받은 표본에서 4번 염색체의 결실이 확인되었다. 염색체 구조이상의 전체 양은 방사선량이 증가함에 따라 증가하는 경향을 보였으며 2 Gy 이상의 피폭을 받은 경우에 급격하게 증가하는 양상이었다. 유전체의 복제수 변화를 수반하지 않는 균형적 구조적 이상은 방사선에 의해 유발되는 특이적인 형태의 구조이상으로 2 Gy 이상의 피폭을 받은 표본에서 높은 빈도로 발견되었다. 표본 내

단일염기서열변이의 양은 췌장 오가노이드 분석의 결과 피폭방사선량의 증가와의 관련성이 낮았으나 이중염기서열변이의 양은 피폭방사선량이 증가함에 따라 증가하는 양상을 보였다. 유전체 내 비반복서열 부위에서 발견되는 작은 크기의 염색체 제거 및 삽입 (indel)은 2 Gy 이상의 방사선 피폭을 받은 표본 내에서 증가하는 양상을 보였다. 군집돌연변이 서열을 토대로 한 체성돌연변이 패턴 (mutational signature) 분석은 C>T의 변이에 특징적인 형태를 보였다. 손상된 DNA 복구 기전과 방사선 유발 손상에 좀 더 특이적인 DNA 손상 복구 기전에 참여하는 유전자들이 방사선 조사 후 2 h 이후에서부터 증가하였다. 방사선에 의해 활성화되는 신호전달 체계에서는 DNA 복구 기전 (NES 1.4, FDR q value 0.060) 뿐만 아니라 Myc 표적 기전 (NES 2.08, FDR q value <0.01)이 활성화되었고 이는 방사선에 의한 유전체 불안정성에 관련이 있을 것으로 추정되었다.

결론:

조직 특이적인 성체줄기세포의 오가노이드 배양을 수행하였고 이를 감마선의 체성돌연변이 유발 평가연구에 적용하였다. 유선조직 유래 성체줄기세포는 췌장 유래 성체줄기세포에 비해 좀 더 방사선 민감성을 보였다. 피폭방사선량이 증가함에 따라 특정한 형태의 염색체 구조변이 (결실, 균형적 구조이상, 복합구조이상)의 양이 증가하였으며 이는 방사선에 의해 유발된 염색체 구조변이임을 시사하였다. 방사선에 피폭된 오가노이드 유전체 내 군집돌연변이의 분석을 통해 방사선에 의해 유발된 mutational signature의 한 형태 (이중뉴클레오티드다형성)를 확인할 수 있었다. 오가노이드를 이용한 방사선 유발 체성돌연변이의 분석을 통해 이후 방사선의 발암유발 기전에 대해 깊이 이해하고 이를 인체 연구에 적용할 수 있는 가능성을 보았다.

주요어: 오가노이드, 성체줄기세포, 감마선, 전장유전체 분석, 체성돌연변이, 염색체, 구조이상

학번: 2015-30714